

Strong Lensing by Galaxies

TOMMASO TREU

Physics Department, University of California, Santa Barbara CA 93106-9530,
 tt@physics.ucsb.edu; Sloan Research Fellow; Packard Research Fellow.

Key Words Gravitational Lensing, Galaxy Evolution, Galaxy Formation, Dark
 Matter, Dark Energy

Abstract Strong lensing is a powerful tool to address three major astrophysical issues: un-
 derstanding the spatial distribution of mass at kpc and sub-kpc scale, where baryons and dark
 matter interact to shape galaxies as we see them; determining the overall geometry, content, and
 kinematics of the universe; studying distant galaxies, black holes, and active nuclei that are too
 small or too faint to be resolved or detected with current instrumentation. After summarizing
 strong gravitational lensing fundamentals, I present a selection of recent important results. I
 conclude by discussing the exciting prospects of strong gravitational lensing in the next decade.

CONTENTS

Introduction 3
 Brief Theoretical Introduction 5
 A gravitational optics primer 5
 Modeling galaxies: macro, milli, and micro lensing 9
 Observational Overview 14
 Present-day samples and challenges 14

<i>Selection</i>	17
The Mass Structure of Galaxies	20
<i>Luminous and dark matter in early-type galaxies</i>	21
<i>Luminous and dark matter in spiral galaxies</i>	29
Substructure in Galaxies and the “Excess Subhalos” Problem	31
<i>Background</i>	31
<i>Possible solutions</i>	32
<i>Flux ratio anomalies</i>	33
<i>Astrometric and time-delay anomalies</i>	36
Cosmography	37
<i>Time delays</i>	38
<i>Lenses as standard masses</i>	43
<i>Compound lenses</i>	44
<i>Lens statistics</i>	45
<i>Is lensing competitive?</i>	46
Lenses as Cosmic Telescopes	47
<i>Small and faint galaxies</i>	47
<i>Host galaxies of lensed active nuclei</i>	48
<i>Structure of active galactic nuclei</i>	49
<i>Cosmic telescopes and human telescopes</i>	51
Searches for Gravitational Lenses	52
<i>Imaging-based searches</i>	53
<i>Spectroscopy-based searches</i>	54
Future Outlook	55
<i>Thousands of gravitational lenses</i>	55
<i>The problem of follow-up</i>	56

<i>Unusual lensing applications in an era of abundance</i>	58
LITERATURE CITED	63

1 Introduction

As photons from distant sources travel across the universe to reach our telescopes and detectors, their trajectories are perturbed by the inhomogeneous distribution of matter. Most sources appear to us slightly displaced and distorted in comparison with the way they would appear in a perfectly homogeneous and isotropic universe. This phenomenon is called weak gravitational lensing (e.g. Refregier 2003, and references therein). Under rare circumstances, the deflection caused by foreground mass overdensities such as galaxies, groups, and clusters is sufficiently large to create multiple images of the distant light source. This phenomenon is called strong gravitational lensing. Due to space limitations, this article will focus on cases where gravitational lensing is caused primarily by a galaxy-sized deflector (or lens).

The first strong gravitational lens was discovered more than thirty years ago, decades after the phenomenon was predicted theoretically (see Blandford & Narayan 1992, and references therein). However, in the past decade there has been a dramatic increase in the number of known lenses and in the quality of the data. At the time of the review by Blandford & Narayan (1992), the 11 “secure” known galaxy-scale lenses could all be listed in a page and discussed individually. At the time of this writing, the number of known galaxy-scale lens systems is approximately 200, most of which have been discovered as part of large dedicated surveys with well defined selection functions. This breakthrough has completed the transformation of gravitational lensing from an interesting and elegant curiosity to a powerful

tool of general interest and statistical power.

Three properties make strong gravitational lensing a most useful tool to measure and understand the universe. Firstly, strong lensing observables - such as relative positions, flux ratios, and time delays between multiple images - depend on the gravitational potential of the foreground galaxy (lens or deflector) and its derivatives. Secondly, the lensing observables also depend on the overall geometry of the universe via angular diameter distances between observer, deflector, and source. Thirdly, the background source often appears magnified to the observer, sometimes by more than an order of magnitude. As a result, gravitational lensing can be used to address three major astrophysical issues: i) understanding the spatial distribution of mass at kpc and sub-kpc scale where baryons and DM interact to shape galaxies as we see them; ii) determining the overall geometry, content, and kinematics of the universe; iii) studying galaxies, black holes, and active nuclei that are too small or too faint to be resolved or detected with current instrumentation.

The topic of strong lensing by galaxies is too vast to be reviewed entirely in a single Annual Review Article. This article is meant to provide an overview of a selection of the most compelling and promising astrophysical applications of strong gravitational lensing at the time of this writing. The main focus is on recent results (after ~ 2005). For each application, I discuss the context, recent achievements, and future prospects. Of course, lensing is only one of the tools of the astronomers' trade. When needed, I discuss scientific results that rely on strong lensing in combination with other techniques. For every astrophysical problem, I also present a critical discussion of whether strong gravitational lensing is competitive with alternative tools.

Excellent reviews and monographs are available to the interested reader for more details, different points of view, history of strong lensing, and a complete list of pre-2005 references. The Saas Fee Lectures by Schneider, Kochaneck and Wambsganss (2006) provide a comprehensive and pedagogical treatment of lensing fundamentals, theory and observations until 2006. Additional information can be found in the review by Falco (2005) and that by Courbin, Saha & Schechter (2002).

The classic monograph by Schneider, Ehlers & Falco (1992) and that by Petters, Levine & Wambsganss (2001) are essential references for strong gravitational lensing theory.

This review is organized as follows. First, for convenience of the reader and to fix the notation and terminology, in § 2 I give a very brief summary of strong lensing theory. Then, in § 3, I present an overview of the current observational landscape. The following four sections cover the main astrophysical applications of gravitational lensing: “The mass structure of galaxies” (§ 4), “Substructure in galaxies” (§ 5), “Cosmography” (§ 6), and “Lenses as cosmic telescopes” (§ 7). After the four main sections, the readers left with an appetite for more results from strong gravitational lensing will be happy to learn about the many promising ongoing and future searches for more gravitational lenses described in § 8. Some considerations on the future of strong gravitational lensing - when the number of known systems should be well into the thousands – are given in § 9.

2 Brief Theoretical Introduction

2.1 A gravitational optics primer

Under standard conditions of a thin lens (i.e. the size of the deflector is much smaller than the distances between the deflector and the observer and the deflector and the source), responsible for a weak gravitational field (i.e. deflection

angles much smaller than unity), in an otherwise homogeneous universe, strong lensing by galaxies can be described as a transformation from the two-dimensional observed coordinates associated with a particular light ray ($\boldsymbol{\theta}$ in the image plane) to the two-dimensional coordinates that the light ray would be observed at in the absence of the deflector ($\boldsymbol{\beta}$ in the source plane).

A simple and intuitive understanding of the basic principles of strong lensing by galaxies can be gained by considering a generalized version of Fermat's principle (Blandford & Narayan 1992, and references therein). For a given source position $\boldsymbol{\beta}$, the excess time-delay surface as a function of position in the image plane is given by:

$$t = \frac{D_d D_s (1 + z_l)}{c D_{ds}} \left(\frac{1}{2} |\boldsymbol{\theta} - \boldsymbol{\beta}|^2 - \psi(\boldsymbol{\theta}) \right), \quad (1)$$

where D_d , D_s , D_{ds} are respectively the angular diameter distances between the observer and the deflector, the observer and the source, and the deflector and the source, and ψ is the two-dimensional lensing potential, satisfying the two-dimensional Poisson Equation:

$$\nabla^2 \psi = 2\kappa, \quad (2)$$

where κ is the surface (projected) mass density of the deflector in units of the critical density $\Sigma_c = c^2 D_s / (4\pi G D_d D_{ds})$ (for convenience of the reader I adopt the same notation as Schneider, Kochanek & Wambsganss 2006).

According to Fermat's principle, images will form at the extrema of the time-delay surface, i.e. at the solutions of the so-called lens equation:

$$\boldsymbol{\beta} = \boldsymbol{\theta} - \nabla \psi = \boldsymbol{\theta} - \boldsymbol{\alpha} \quad (3)$$

which is the desired transformation from the image plane to the source plane.

The scaled deflection angle α is related to the deflection angle experienced by a light ray $\hat{\alpha}$ by $\alpha = \frac{D_{ds}\hat{\alpha}}{D_s}$. The lensing geometry is illustrated in Figure 1. Note that the transformation is achromatic and preserves surface brightness.

Strong lensing occurs when Equation 3 has multiple solutions corresponding to multiple images. Examples of the most common configurations of strong gravitational lensing by galaxies are shown in Figure 2 and explained with an optical analogy in Figure 3. For a given deflector the solid angle in the source plane that produces multiple images is called the strong-lensing cross section. For a given population of deflectors, the optical depth is the fraction of the sky where distant sources appear to be multiply-imaged.

The Jacobian of the transformation from the image to the source plane, gives the inverse magnification tensor, which can be written as

$$\frac{\partial \beta}{\partial \theta} = \delta_{ij} - \frac{\partial^2 \psi}{\partial \theta_i \partial \theta_j} = \begin{pmatrix} 1 - \kappa - \gamma_1 & -\gamma_2 \\ -\gamma_2 & 1 - \kappa + \gamma_1 \end{pmatrix} \quad (4)$$

and describes the local isotropic magnification of a source (determined by the convergence κ , defined above) and its distortion (shear components γ_1 , and γ_2).

In the limit of a point source, the local magnification μ is given by the determinant of the magnification tensor:

$$\mu = \frac{1}{(1 - \kappa)^2 - \gamma_1^2 - \gamma_2^2}. \quad (5)$$

For extended sources, the observed magnification depends on the surface brightness distribution of the source as well as on the magnification matrix.

When the determinant of the inverse magnification matrix vanishes, the magnification becomes formally infinite. The loci of formally infinite magnification in the image plane are called critical lines. The corresponding loci in the source plane

are called caustics. Compact sources located close to a caustic can be magnified by very large factors up to almost two orders of magnitude (Stark et al. 2008), although the total observed flux is always finite for astrophysical sources of finite angular size.

It is convenient to define the Einstein radius. For a circular deflector it is the radius of the region inside which the average surface-mass density equals the critical density. A point source perfectly aligned with the center of a circular mass distribution will be lensed into a circle of radius equal to the Einstein radius, the so-called Einstein ring (see Figure 2). The size of the Einstein radius depends on the enclosed mass as well as on the redshifts of deflector and source. The definition of Einstein radius needs to be modified for non-circular deflectors (Kormann, Schneider & Bartelmann 1994). Once appropriately defined, the Einstein radius is a most useful quantity to express the lensing strength of an object, and it is usually very robustly determined via strong lens models (e.g. Schneider, Kochanek & Wambsganss 2006). As a consequence, the mass enclosed in the cylinder of radius equal to the Einstein radius can be measured to within 1-2%, including all random and systematic uncertainties.

A final essential concept is that of mass-sheet degeneracy (Falco, Gorenstein & Shapiro 1999). Given dimensionless observables in the image plane, such as relative position, shape, and flux ratios of multiple images, the solution of the lens equation is not unique. For every mass distribution $\kappa(\boldsymbol{\theta})$ and every surface brightness distribution in the source plane $I(\boldsymbol{\beta})$, there is a family of solutions given by the transformations:

$$\kappa_\lambda = (1 - \lambda) + \lambda\kappa; \quad \boldsymbol{\beta}_\lambda = \boldsymbol{\beta}/\lambda. \quad (6)$$

The transformation changes the predicted time-delay between multiple images

and the magnification as follows:

$$\Delta t_\lambda = \Delta t / \lambda; \quad \mu_\lambda = \mu / \lambda^2, \quad (7)$$

resulting in a degeneracy in inferred quantities such as intrinsic luminosity and size of the background source. Additional information is needed to break this degeneracy, such as the intrinsic luminosity or size of the lensed source (as in the case of lensed supernovae Ia Kolatt & Bartelmann 1998), the actual mass of the deflector (as measured for example with stellar kinematics), or the measured time-delays between multiple images within the context of fixed cosmology. Alternatively, the mass-sheet degeneracy can be broken in the context of a model, for example by assuming that the surface mass density of the deflector goes to zero at large radii (thus $\lambda = 1$). In practice, this is not always possible because mass structure along the line of sight - associated or not with the main deflector - can act effectively as a “sheet” of mass with external convergence κ_{ext} . Breaking the mass-sheet degeneracy is essential for a number of strong lensing applications, as we will see in Section 6.

2.2 Modeling galaxies: macro, milli, and micro lensing

It is useful to define three regimes to describe the lensing properties of the components of galaxies, corresponding to the typical scale of associated Einstein radii, as summarized in Figure 4.

2.2.1 MACROLENSING On the coarsest scale, corresponding to Einstein radii of the order of arcseconds, the overall mass distribution of the lensing galaxy is responsible for the main features of the multiple images, such as image separation and multiplicity. In terms of physical components of an isolated galaxy, macrolensing can be thought of as the combined lensing properties of the DM

halo, the bulge, and the disk. A simple model that reproduces image positions, multiplicity, and fluxes is sometimes referred to as the macro model, and is generally sufficient to infer quantities such as projected mass inside the Einstein radius and overall ellipticity and orientation of the mass distribution. The simplest model that is found to provide a qualitatively good description of the macroscopic features of strong lensing by galaxies is the SIE (Kormann, Schneider & Bartelmann 1994), an elliptical generalization of the SIS. The three-dimensional mass density profile of the SIS is given by

$$\rho = \frac{\sigma_{\text{SIS}}^2}{2\pi G r^2}, \quad (8)$$

and the Einstein radius is given by

$$\theta_E = 4\pi \left(\frac{\sigma_{\text{SIS}}}{c} \right)^2 \frac{D_{ds}}{D_s}. \quad (9)$$

Note that for early-type lens galaxies σ_{SIS} is found to be approximately equal to the stellar velocity dispersion (e.g., Bolton et al. 2008a).

An example lens model is shown in Figure 5. This system consists of a foreground elliptical galaxy lensing a background galaxy, well described by an elliptical Gaussian surface brightness distribution in the source plane. A SIE mass model is found to be sufficient to reproduce accurately the observed surface brightness distribution in the image plane. For an SIE mass model, two curves (outlined in white in the figure) separate regions of different multiplicity in the source plane. Sources outside the outer curve (known as cut) are singly imaged, sources in between the cut and the inner caustic curve produce two visible images (plus a third infinitely demagnified central image), and sources inside the inner caustic produce four visible images (plus a fifth infinitely demagnified central

image). In this case, the detectable part of the extended source crosses the inner caustic so that it appears partly doubly-imaged and partly quadruply imaged. Due to the good alignment of the deflector and source, the image forms an almost perfect Einstein ring. An alternative light traces mass (LTM) model (i.e. the surface mass density of the deflector is obtained by multiplying its surface brightness by a mass-to-light ratio, allowed to be a free-parameter) is also shown. In this case, the LTM model is almost indistinguishable from an SIE model, because strong lensing is sensitive only to the mass enclosed by the Einstein radius, to first order. In general, LTM models can be excluded when considering extended sources because they fail to reproduce the detailed geometry, the radial behavior in particular. LTM models can also be excluded on the basis of a number of other considerations, as reviewed in § 4.

We just discussed an example of a simply-parametrized gravitational lens macro model, where both the source surface brightness and the mass distribution of the deflector are described by astrophysically motivated models with a small number of parameters. This kind of model is generally capable of reproducing all the macroscopic features while delivering robust estimates of the most important quantities for the deflector (e.g. total mass ellipticity and orientation) and the source (e.g. intrinsic size and luminosity). For these reasons, simply parametrized models are often all one needs in interpreting lensing data.

However, some applications require more sophisticated lens models, capable of extracting more detailed information. In recent years, the increase in number of known lenses has been paralleled by ever more sophisticated lens modeling tools. A full description of advanced lens models is beyond the scope of this review. However, I list a few examples to point the interested reader towards the tech-

nical literature. A number of groups have developed “grid-based” models (also known – incorrectly – as non-parametric models; pixel values are parameters like any other), where the potential (or surface mass density) of the deflector and/or the surface brightness of the source are described by a set of pixels on regular or irregular grids, using regularization schemes to suppress spurious features due to noise (e.g. Brewer & Lewis 2006, Dye & Warren 2005, Koopmans 2005, Suyu et al. 2006, Treu & Koopmans 2004, Vegetti & Koopmans 2009a, Warren & Dye 2003).

An alternative hybrid approach consists of using large numbers of simply-parametrized models to strike a balance between flexibility and prior information on the shape and surface brightness of galaxies (Marshall 2006). Bayesian statistics has become the standard statistical framework for advanced models, allowing for rigorous analysis of the uncertainties in highly dimensional spaces as well as quantitative model selection. Heuristic pixellated approaches have also been adopted with some success (Saha & Williams 2004), and recently been cast in a Bayesian framework to improve the understanding of the uncertainties (Coles 2008).

2.2.2 MILLILENSING On an intermediate angular scale are the lensing effects introduced by substructure, both luminous and dark. Typically, a lens galaxy will have some satellites, like the dwarf satellites of the Milky Way (Kravtsov 2010, and references therein). The mass associated with the satellites introduces perturbations in an otherwise smooth potential. These perturbations can be detected relative to a smooth model using accurate measurements of flux ratios, relative position, and time delays between multiple images. This regime is sometimes referred to as millilensing – due to the characteristic milli-arcsecond Einstein radii expected for dwarf satellites of massive galaxies. However, the phenomenon could span several orders of magnitude, depending on the mass function of satellites

and their spatial distribution (e.g. Kravtsov 2010).

2.2.3 MICROLENSING Finally, on the smallest angular scale, galaxies are made of stars. The Einstein radius of a solar mass star at a cosmological distance is of the order of micro arcseconds, hence the name cosmological microlensing. The average projected separation of stars in distant galaxies is small compared to the typical Einstein radii, and thus every background source effectively experiences cosmological microlensing. As in the case of galactic microlensing, the resolution of current instruments is insufficient to detect cosmological microlensing via astrometric effects. However, if the angular size of the background source is smaller or comparable to the typical stellar Einstein radius, cosmological microlensing can be detected by its effect on the observed flux. In contrast, if the source is much larger than the typical stellar Einstein radius, the total magnification will be effectively averaged over a large portion of the magnification pattern and therefore be similar to that expected for a smooth model. The relative motion of stars with respect to the background source and center of mass of the deflector are sufficiently fast to modify the magnification pattern over timescales of just a few years, as illustrated in Figure 6.

As we will see in the rest of this article, all three regimes can be used to infer unique information on the distribution of mass in (deflector) galaxies, and on the surface brightness distribution of distant (lensed) galaxies and active galactic nuclei with sensitivity and resolution beyond those attainable without the aid of gravitational lensing.

3 Observational Overview

3.1 Present-day samples and challenges

Approximately 200 examples of strong gravitational lensing by galaxies have been discovered to date. A number of different strategies have been followed. The two most common strategies start from a list of potential sources or potential deflexors and use additional information to identify the (small) subset of strong gravitational lensing events. Other promising approaches include searching for gravitational lensing morphologies in high resolution data (Marshall et al. 2009, and references therein) and exploiting variability in time domain data (Kochanek et al. 2006a). The current state of the art is illustrated in Figure 7, which shows the redshift distribution of the lenses discovered by the four largest surveys to date. The first two are source-based surveys, the third is a deflector-based survey, and the fourth one is a lensing morphology survey.

The Cosmic Lens All-Sky Survey (CLASS) is based on radio imaging. They discovered 22 multiply-imaged active nuclei, including a subset of 13 systems which are known as the statistically well-defined sample (Browne et al. 2003). Source and deflector redshifts are available for 11 and 17 systems, respectively (C.D.Fassnacht, 2009 priv. comm). The SDSS Quasar Lens Search (SQLS), identified 28 galaxy-scale multiply-imaged quasars using SDSS multicolor imaging data to sift through the spectroscopic quasar sample (Oguri et al. 2006, 2008). All source redshifts are available, while deflector redshifts are available for 15 systems. The SLACS Survey (Bolton et al. 2006) is an optical survey based on spectroscopic preselection from SDSS data and imaging confirmation with HST. SLACS discovered 85 galaxies acting as strong lenses (plus an additional 13 prob-

able lenses; Auger et al. 2009). Source and deflector redshifts are available for all systems. Finally, twenty secure galaxy-scale lens systems were discovered by visual inspection (Faure et al. 2008, Jackson 2008) of the HST images taken as part of the COSMOS Survey. Source and deflector redshifts are available for 3 and 13 systems, respectively (Lagattuta et al. 2009).

The compilation is not complete, due to the difficulty of keeping track of the ever growing number of lenses discovered serendipitously or by ongoing concerted efforts (Cabanac et al. 2007, Marshall et al. 2009) that still lack confirmation and spectroscopic redshifts (a useful resource to find data for lenses from a variety of sources is the online database of strong gravitational lenses CASTLES at URL <http://www.cfa.harvard.edu/castles>). However, the compilation gives a good idea of the observational landscape and of the two main limitations of current samples. Firstly, most new lenses have been found at $z \lesssim 0.4$, which is a very favorable regime for detailed follow-up, but limits the look-back time baseline for evolutionary studies and the spatial scales probed by lensing. Secondly, many gravitational lens systems still lack source or deflector redshifts.

It is customary to classify strong lenses as galaxy-galaxy lenses (e.g. Figs 2 and 5), and galaxy-QSO lenses (e.g. Figure 6), depending on whether an active galactic nucleus is present in the background source. Galaxy-QSO lenses are more rare on the sky than galaxy-galaxy lenses (Marshall, Blandford & Sako 2005). However, they can be found efficiently by exploiting their radio emission and the variability of the point source. Furthermore, the compact point source enables studies of the granularity of the lens galaxy (from microlensing), and of cosmography and lens galaxy structure (from direct measurements of time delays between images). Galaxy-galaxy lenses are typically more suited for the study

of the lens galaxy itself, because its emission is not overwhelmed by the multiple images of the background source. Furthermore, the extended surface brightness of the source provides detailed information on the gravitational potential of the deflector.

It is observationally challenging to extract the wealth of information available from strong lensing systems. First and foremost, subarcsecond angular resolution is key to identifying and characterizing strong lensing systems. Radio or optical/near infrared observations from space (and recently from the ground with adaptive optics) have been essential for the progress of the field. Secondly, both source and deflector redshifts are needed to transform angular quantities into masses and lengths. Especially for the source redshift, long exposure on the largest telescopes are typically required (e.g. Ofek et al. 2006). Success is not assured, and in many cases one must rely on photometric redshifts, which are also challenging because light from the foreground deflector complicates photometry of the background source. Third, microlensing and variability depend critically on source size. This makes X-ray (e.g., Pooley et al. 2009) and mid-infrared observations (e.g., Agol et al. 2009) – probing sources that are much smaller and much larger than the scale of microlensing, respectively – particularly useful, even with limited spatial resolution. Fourth, time delays and microlensing studies require intensive monitoring campaigns, with all the associated logistical challenges. Lastly, depending on the application, ancillary data such as velocity dispersion or information on the local large scale structures are typically needed to break degeneracies and control systematic errors.

3.2 Selection

Strong lensing is a very rare phenomenon. With present technology only $\sim 1/1000$ galaxies can be detected as strong lenses (Marshall, Blandford & Sako 2005). Similarly, the optical depth is of order 10^{-3} - 10^{-4} , i.e. $\lesssim 1/1000$ high-redshift sources in the sky have detectable multiple images (e.g. Browne et al. 2003). Both numbers depend strongly on the depth of the observations. Thus, in order to generalize the results obtained from this technique to the overall population of deflectors and sources, and for applications of strong lensing to cosmography, it is essential to understand the selection function very well.

To first order, strong lensing galaxies can be described as selected by velocity dispersion. Most galaxy-scale strong gravitational lenses discovered to date are massive elliptical galaxies with velocity dispersions in the range 200-300 km s^{-1} . This well-understood selection function arises from the rapid increase in the strong lensing cross section with mass ($\propto \sigma^4$ for an SIS), and from the rapid decline of the velocity dispersion function of galaxies above 300 km s^{-1} (see Schneider, Kochanek & Wambsganss 2006, for a comprehensive discussion). As an example, the average stellar velocity dispersion of the SLACS sample is 248 km s^{-1} with a r.m.s. scatter of 46 km s^{-1} . The velocity dispersion selection is also responsible for the adverse selection against late-type galaxies. Approximately 80% of the SLACS deflectors are pure ellipticals, 10% are lenticulars and 10% are spirals, mostly bulge dominated (Auger et al. 2009). Identifying and studying galaxies with $\sigma \lesssim 200 \text{ km s}^{-1}$ acting as strong gravitational lenses is possible with sufficiently large surveys and represents an exciting frontier for the next decade. However, this is an observationally challenging problem because the image separation drops quickly below $0''.3 - 0''.4$, the current practical limit

for detection with HST and the Very Large Array (VLA). Furthermore, once the resolution drops significantly below the typical arcsecond size of distant galaxies, disentangling light from the deflector and background source becomes increasingly difficult, particularly at optical/infrared wavelengths.

The lensed sources are to first order flux and surface brightness selected. This translates into a complex selection function in terms of the intrinsic properties of the source population because of the magnification effects of lensing. It is easier to understand the effect for point source surveys, such as CLASS and SQLS. Due to lensing magnification, sources that are fainter than the survey flux limit will enter the sample. However, magnification also reduces the solid angle actually surveyed. Therefore, the number of strong lensing events depends critically on the dependency of the surface density of sources on the observed flux. This effect is known as magnification bias. For extended sources, observed magnification will also depend on surface brightness and size of the source, generally being larger for more compact sources. The redshift distribution of the lensed sources will in general be different than that for a non-lensed population selected to the same apparent magnitude limit.

Other more subtle selection effects are also at work. Factors that may affect the strong lensing cross-section of a galaxy include elongation along the line of sight, flattening of the projected mass distribution, concentration of the mass distribution (e.g., the slope of the mass density profile at fixed virial mass), overdensity of the local environment, and abundance of small scale structure in the plane of the deflector or along the line of sight. Factors that may affect the probability of a source being identified as multiply-imaged include extinction from the foreground lens galaxy, configuration of the multiple images (in particular

image separation and flux ratios), time variability, and presence of emission lines and hence properties of the stellar populations or existence of an active nucleus.

Three complementary strategies have been followed to quantify selection effects. One strategy consists of starting from a realistic cosmological model and simulating the selection process from first principles (e.g. Mandelbaum, van de Ven & Keeton 2009, and references therein). This is the most direct way to compare observations with theoretical models of galaxy formation. The challenge of this approach is that lensing selection depends on the details of the mass and surface brightness distributions on scales much smaller than a galaxy. Unfortunately, realistic simulations of the universe on this scale are beyond our current capabilities. Therefore, one needs to rely on DM-only simulations and approximate the effects of baryons, with all associated uncertainties. A second strategy consists of comparing samples of lens galaxies with control samples of non-lens galaxies. This approach was used with the SLACS sample to show that – once velocity dispersion and redshifts are matched – lens galaxies are indistinguishable within the uncertainties from twin galaxies selected from SDSS in terms of their size, surface brightness, luminosity, location on the fundamental plane, stellar mass, and local environment (Auger et al. 2009, Bolton et al. 2008a, Treu et al. 2009, 2006). This finding implies that the results from the SLACS Survey can be applied to the overall population of velocity dispersion selected early-type galaxies. The strength of this method is its ability to take into account real selection functions with all the inherent complexity. This guarantees that one compares apples with apples, but does not solve the problem of comparing with theoretical models. A “hybrid” approach consists of constructing simple models starting from empirically-based information on the deflector and source populations, and combining it with lens-

ing theory to compute the relevant selection function. This approach is extremely useful for developing an intuition for the process and compute approximate correction factors. For example, Oguri (2007) was able to explain the observed ratio of quadruply imaged to doubly imaged quasars in the CLASS sample in terms of magnification bias. The challenge for this approach is including a sufficiently accurate description of the physics and details of the observations to infer quantitatively correct answers.

4 The Mass Structure of Galaxies

The standard cosmological model, based on CDM and dark energy reproduces very well the observed structure of the universe on supergalactic scales (e.g., Komatsu et al. 2009, and references therein). At galaxy scales, DM and baryons interact to produce the observed variety of galaxy properties. The situation is not so clear at small sub-galactic scales, where potential conflicts between theory and observations have been suggested (e.g. Ellis & Silk 2009). Understanding the interplay between DM and baryons is crucial to make progress in developing and testing theories of galaxy formation at these scales. Gravitational lensing, by providing direct and precise measurements of mass at galactic and subgalactic scales, is a fundamental tool for answering a number of questions with profound implications on the existence and nature of DM. Do galaxies reside in DM halos? How do the properties of galaxies depend on those of their DM halos? Are DM density profiles universal as predicted by simulations? These are the topics of this section.

4.1 Luminous and dark matter in early-type galaxies

4.1.1 DO EARLY-TYPE GALAXIES LIVE IN DARK MATTER HALOS? It is commonly believed that all galaxies live in DM halos. However, in the case of early-type galaxies, observational evidence is hard to obtain. The difficulty arises mostly from the paucity of mass tracers at radii much larger than the effective radius R_e – where DM dominates – and from the degeneracies inherent in interpreting projected data in terms of a three-dimensional mass distribution for pressure supported systems. Chief among these degeneracies is that between the total mass density profile and the anisotropy of the pressure tensor (“mass-anisotropy” degeneracy, e.g., Treu & Koopmans 2002a).

Much progress in detecting DM halos has been achieved by studying the kinematics of stars, globular clusters, and cold and hot gas in nearby systems (e.g., Bertin & Stiavelli 1993, Humphrey et al. 2006). This type of study shows that DM halos are generally required to explain the dynamics of massive early-type galaxies. Weak-lensing has been used to demonstrate the existence and to characterize the outer regions of DM halos for statistical samples of early-type galaxies out to intermediate redshifts ($z \sim 0.5$, e.g. Gavazzi et al. 2007, Hoekstra et al. 2005, Lagattuta et al. 2009).

Strong lensing observations demonstrate the existence of DM halos around individual massive early-type galaxies out to $z \sim 1$ beyond any reasonable doubt, both by themselves and in combination with other techniques (for early-type galaxies with $\sigma \lesssim 200 \text{ km s}^{-1}$ the case is much less conclusive; future sample of low-mass deflectors may be needed to clarify matters). One argument is that the amount of mass inside the Einstein radius exceeds the stellar mass M_* . This latter quantity can be constrained in many ways. Assuming an IMF, stellar population

synthesis (SPS) models applied to photometric or spectroscopic data yield M_* with an uncertainty of 0.1-0.2 dex. Alternatively, local dynamical studies of early-type galaxies (Cappellari et al. 2006, Gerhard et al. 2001) constrain the stellar mass-to-light ratio at present time, which can then be evolved back in time either using the measured evolution of the fundamental plane or other measurement of the star formation history (e.g., Kochanek 1995, Treu & Koopmans 2004).

A particularly powerful combination for detecting DM halos is to use stellar kinematics of the lens galaxy to provide information on the distribution of mass in the high surface brightness regions well within the effective radius, and to use strong lensing to help remove the mass-anisotropy degeneracy (e.g. Barnabè et al. 2009, Treu & Koopmans 2004). A third method relies on assuming scaling relations to analyze lenses across a sample and reconstruct the mass density profile for the ensemble, which turns out to be more extended than expected if mass followed light and therefore consistent with DM (Bolton et al. 2008b, Rusin & Kochanek 2005). A fourth method exploits microlensing statistics to demonstrate that point masses (i.e. stars) cannot contribute the totality of the surface mass density at the location of the multiple images (e.g. Pooley et al. 2009). A fifth method consists of measuring time delays between multiple images, determining angular-diameter distances from independent cosmographic probes to infer the behavior of the mass density profile at the location of the multiple images (Kochanek et al. 2006b).

4.1.2 WHAT IS THE RELATIVE SPATIAL DISTRIBUTION OF LUMINOUS AND DARK MATTER? The efficiency with which baryons condense inside halos to form stars, and their effect on the underlying DM distribution, depend on the interplay between cooling and heating (e.g. from star formation and nuclear

activity). Lensing can help us understand these process by providing precise measurements of the fraction of total mass in the form of DM (f_{DM}) within a fixed projected radius, typically expressed in terms of fraction of the effective radius (e.g. Jiang & Kochanek 2007).

Observationally, f_{DM} is found to be non-negligible already at the effective radius ($25 \pm 6\%$ Koopmans et al. 2006) and increasing towards larger radii ($70 \pm 10\%$ at five effective radii Treu & Koopmans 2004). Consistent results are obtained by a number of independent non-lensing techniques (e.g. Cappellari et al. 2006). In addition, f_{DM} within a fixed fraction of the effective radius is found to increase with galaxy stellar mass and velocity dispersion. For example, by comparing lensing masses with those inferred from SPS modeling of multicolor data, f_{DM} inside the cylinder of projected radius equal to the Einstein radius increases from $\sim 25\%$ to $\sim 75\%$ in the range of velocity dispersion $\sigma = 200\text{--}350 \text{ km s}^{-1}$, or equivalently in the range of stellar mass between 10^{11} and $10^{12} M_{\odot}$ (Auger et al. 2009, Figure 8). These numbers are based on a Salpeter (1955) IMF and are consistent with those inferred by local dynamical studies (e.g. Cappellari et al. 2006). Adopting a Chabrier (2003) IMF changes the overall normalization, but not the global trend (Auger et al. 2009, see, however, Grillo et al. 2009 for a contrasting view).

Strong lensing studies also explain the origin of the so-called tilt of the fundamental plane (e.g., Ciotti, Lanzoni & Renzini 1996, hereafter FP), the tight correlation between effective radius, effective surface brightness and stellar velocity dispersion observed for early-type galaxies. By introducing a dimensional mass variable $M_{\text{dim}} \equiv \sigma^2 R_e / G$, the FP can be cast in terms of an increasing effective mass-to-light ratio with effective mass (the tilt'). Exploiting strong lensing, a

somewhat tighter mass plane (MP Bolton et al. 2008b) relation can be obtained by replacing surface brightness with total surface mass. The MP is not tilted, implying that the tilt of the FP stems from an increase in f_{DM} with mass, and not in a systematic change, e.g., of the virial coefficient that connects M_{dim} to total mass.

4.1.3 MASS DENSITY PROFILES AND THE BULGE-HALO CONSPIRACY Another quantity of interest is the average logarithmic slope of the three-dimensional total mass density profile $d \log \rho_{\text{tot}} / d \log r \equiv -\gamma'$. An isothermal mass model has $\gamma' = 2$. The total mass density profile for a spherical model is often expressed in terms of the equivalent circular velocity

$$v_c \equiv \sqrt{\frac{GM(< r)}{r}}, \quad (10)$$

which facilitates comparison with the literature on spiral galaxies and on numerical simulations. For a spherical power-law density profile, γ' is simply related to the slope of the rotation curve by the relation $d \log v_c / d \log r = (2 - \gamma')/2$. For this reason, an isothermal profile is sometimes referred to as a flat rotation curve.

The basic result on this topic is that $\gamma' \approx 2$, i.e. early-type lens galaxies have approximately isothermal mass density profiles, or close-to-flat equivalent rotation curves. This has been known since at least the early nineties, both on the basis of lensing studies (e.g. Kochanek 1995) and on local kinematics (e.g. Bertin & Stiavelli 1993, Gerhard et al. 2001, and references therein). However, in order to understand the mass structure of galaxies with sufficient level of precision to constrain formation models, we need to ask more detailed questions. What is the average γ' and its intrinsic scatter for the overall population of early-type galaxies? How does γ' depend on the galactic radius or other global properties? Does it depend on the environment, as expected if halos were tidally truncated?

Does γ' evolve with redshift? In addition, as we will see in § 6, determining the mass profiles of lens galaxies to high accuracy is essential for many applications to cosmography.

In the past few years, the large number of lenses discovered and the high level of precision attainable with lensing has enabled substantial breakthroughs. Joint lensing and dynamical studies of the SLACS sample have shown that $\gamma' = 2.08 \pm 0.02$ with an intrinsic scatter of less than 10% (Koopmans et al. 2009b). This result is valid in the sense of an average slope inside one effective radius or less, the typical size of the Einstein radius of SLACS lenses. For higher redshift deflectors, Einstein radii are typically larger than the effective radius and reach out to $5 R_e$. Although the high redshift samples with measured velocity dispersions are small, they seem to suggest a somewhat larger intrinsic scatter around $\gamma' = 2$ (Treu & Koopmans 2004). No significant dependency on galactic radius, global galaxy parameter, or redshift has been found so far based on lensing and dynamical analysis (Koopmans et al. 2009b). The small scatter around $\gamma' = 2$ is remarkable, considering that neither the DM halo, nor the stellar mass are well described by a simple power-law profile. Nevertheless, the two components add up to an isothermal profile (Fig. 9). This effect is similar to the disk-halo conspiracy responsible for the flat rotation curves of spiral galaxies (van Albada & Sancisi 1986), and it is therefore been dubbed the 'bulge-halo conspiracy'. Detailed dynamical studies of the twodimensional velocity field of deflector galaxies in conjunction with strong gravitational lensing confirm this picture to higher accuracy (Barnabè et al. 2009).

Similar and consistent results can be obtained directly from gravitational lens models, both for lensed sources covering a significant radial range (e.g. Dye & Warren 2005)

or when a gravitational time delay has been measured and the cosmology is fixed by independent measurements (Kochanek et al. 2006b). An interesting case is that of the system SDSSJ0946+1006 where the presence of two multiply-imaged sources at different redshifts constrains the projected mass density slope to be $\gamma' = 2.00 \pm 0.03$, based purely on lens modeling (Figure 10). The lack of central images also constrains the slope of the total density profile to be steep (e.g., $\gamma' = 2$) in the central regions of deflectors. It should be noted that lensing is mostly sensitive to the projected mass density slope at the location of the images, rather than the average inside the images. Therefore, a direct comparison with the lensing and dynamical results is only valid to the extent that a pure power-law profile is a good model for the data.

4.1.4 ARE DARK MATTER DENSITY PROFILES UNIVERSAL? Cosmological numerical simulations predict that DM density profiles should be almost universal in their form (Navarro, Frenk & White 1997, hereafter NFW). Simulated profiles are characterized by an inner slope $d \log \rho_{DM} / d \log r = -\gamma \approx -1$. At the scales of spiral galaxies, low surface brightness galaxies, and clusters of galaxies, it has been shown that in a number of systems the observed profiles are shallower than predicted (i.e. $\gamma < 1$, e.g., Salucci et al. 2007, Sand et al. 2008). The discrepancy suggests that either the DM component or the effects of baryons on the underlying halos are poorly understood.

In early-type galaxies the inner regions are completely dominated by stellar mass, making them particularly interesting systems for understanding the interplay between baryons and DM. Unfortunately, the dominance of baryons also makes the measurement more challenging. A joint lensing and dynamical analysis of 5 high- z lenses shows that γ is consistent with unity, albeit with large errors,

and shallower slopes cannot be excluded (Treu & Koopmans 2004). Improving the measurement will require larger samples of objects with good quality data and further constraints on the stellar mass-to-light ratio.

Alternatively, by imposing $\gamma = 1$ one can infer an absolute normalization of the stellar mass component, and thus constrain the IMF of massive early-type galaxies to be close to Salpeter (Grillo et al. 2009, Treu et al. 2010). A joint lensing, dynamical, and stellar population analysis of the SLACS sample shows that massive early-type galaxies cannot have both a universal DM halo and universal IMF (Treu et al. 2010): either the inner slope of the DM halo or the normalization of the IMF have to increase with deflector velocity dispersion.

4.1.5 IMPLICATIONS FOR EARLY-TYPE GALAXY FORMATION Massive early-type galaxies are simple dynamical systems with simple stellar populations. Yet, their formation and evolution is still far from being well understood (for a comprehensive review see S.M. Faber, this volume). The standard CDM model postulates their formation via major mergers, but this is hard to reconcile with their uniformly old stellar populations – unless there is some fine-tuned feedback mechanism that prevents star formation in the high mass systems (see Renzini 2006, for a recent review) – and with the slow observed evolution of their stellar mass function since $z \sim 1$. Recently, collisionless mergers not involving gas and star formation (and therefore “dry”) have become increasingly popular as a possible mechanism of growth (Faber, this volume). Furthermore, dry mergers can grow galaxies in size faster than in velocity dispersion. Therefore they have been suggested as a possible mechanism for the evolution of ultradense massive galaxies at high redshift into the more diffuse ones found in the local universe (van der Wel et al. 2009).

Strong lensing studies give us some direct information on the connection between baryons and DM, and therefore offer us new insights into this problem. The (non-evolving) isothermality of the total mass density profile requires an early dissipative phase, to steepen the NFW profiles predicted in CDM-only simulations. Alternatively, an initial collapse associated with incomplete violent relaxation could have established the isothermality of the inner profiles. Either phenomenon must have occurred well before $z \sim 1$. After the initial formation, further growth by dry mergers preserves the isothermal profile and tightness of the mass plane (Koopmans et al. 2006; Nipoti, Treu & Bolton 2009). However, dry mergers do not preserve the tight correlations between size and total mass and velocity dispersion and total mass (Nipoti, Treu & Bolton 2009). The observed tightness of the correlation limits the growth by dry mergers to have been at most a factor of two since $z \sim 2$, unless there is a large degree of fine tuning between orbital parameters of the merger and location in the size-mass-velocity dispersion space. Therefore, it seems most likely that the majority of the mass assembly must have occurred during the initial dissipative phase associated with the dominant episode of star formation.

The other main strong lensing result, i.e. the correlation between DM fraction and velocity dispersion (stellar mass), provides us with another piece of the puzzle. Dry mergers increase f_{dm} (Nipoti, Treu & Bolton 2009), thus creating part of the trend. However, dry-mergers cannot explain the whole trend, which must be largely established early-on through other means. A scenario where the time since major initial collapse increases with present-day mass could explain the trend in terms of the evolution of the density of the universe with cosmic time (Thomas et al. 2009). The correlation between present day mass and epoch of

major mass assembly could also help explain the correlations between present day mass, age, and chemical composition of the stellar populations (Treu et al. 2005).

It should be noted that the conclusions above hold only for the most massive early-type galaxies. At lower masses, evolution is certainly more recent and other secular or environmentally driven mechanisms could be responsible for forming early-type galaxies (e.g. Bundy, Treu & Ellis 2007).

4.2 Luminous and dark matter in spiral galaxies

Massive DM halos around local spiral galaxies are readily detected from the gas kinematics at large radii (van Albada & Sancisi 1986). The total gravitational potential can be reconstructed accurately from the observed velocity field. However, decomposing the total mass distribution into its baryonic and dark components for individual galaxies is still an unsolved problem, largely because the stellar mass-to-light ratio is uncertain by a factor of ~ 2 -3 for young and dusty stellar populations. In the distant universe, the problem is compounded by observational difficulties: HI becomes prohibitively expensive to detect; optical rotation curves can be measured out to $z \sim 1$ but are limited by cosmological surface brightness dimming as well as angular resolution. One approach consists of assuming that the baryonic component is maximally important, the so-called maximum-disk ansatz (van Albada & Sancisi 1986). However, it is not clear that disks are indeed maximal. Indeed, submaximal disks seem to be suggested by a variety of arguments (e.g. Courteau & Rix 1999), even though the unknown IMF is a dominant source of uncertainty (Bell & de Jong 2001). Understanding the relative mass in disks and halos is critical to formulate and test a robust theory of disk galaxy formation (e.g. Dutton et al. 2007).

Gravitational lensing provides a new tool for luminous and dark matter decomposition in spiral galaxies. Two factors make lensing particularly useful in this respect. Firstly, it measures the total projected mass within a cylinder. This can then be combined with the enclosed mass in 3D inferred from disk kinematics to break the disk-halo degeneracy by exploiting the different radial dependency of the two components (e.g., Maller, Flores & Primack 1997). Secondly, gravitational lensing provides azimuthal information which also helps pin down the relative contribution of the two, especially if they are misaligned.

Strong lensing studies of spiral galaxies have shown encouraging results, although the impact of the conclusions is limited by the small size of current samples. For example, Trott et al. (2010) combined lensing constraints, high resolution imaging data, and optical and radio kinematics to decompose the mass profile of the Einstein Cross lens galaxy into its bulge, disk, and halo components (see also van de Venn et al. 2010, submitted to ApJ). The mass-to-light ratio of the bulge is very well constrained ($M/L_B = 6.6 \pm 0.3$ in solar units). Due to the unusually small Einstein radius of this system, the mass of the disk is less well constrained, although it is clearly sub-maximal, contributing $45 \pm 11\%$ of rotational support at 2.2 scale lengths.

The situation is changing rapidly, due to progress in strong lensing searches. SLACS discovered approximately 7 new bulge-dominated spiral lenses and an ongoing search based on a similar strategy (SWELLS; HST-GO-11978) should find as many edge-on late type spirals. Dedicated searches (e.g., Féron et al. 2009, Marshall et al. 2009) should discover tens of new systems in the next few years. At variance with the smoothness of early-type galaxies, the small-scale structure of the surface brightness of the spiral lens due to dust and inhomogeneous stel-

lar populations complicates the identification and modeling of multiply-imaged parts of the background source. High resolution near-infrared images with adaptive optics or with HST and JWST, coupled with multicolor optical data, or in the radio, will be essential to make progress on this front (Fig. 11).

5 Substructure in Galaxies and the “Excess Subhalos” Problem

5.1 Background

In the standard cosmology, DM halos host a hierarchy of sub-halos, also known as DM substructure. The number of subhalos above a given mass scales approximately as the total mass of the parent halo, and the logarithmic slope of the subhalo mass function is approximately $dN/dM_{\text{sub}} \propto M_{\text{sub}}^{-\alpha}$, with $\alpha = 1.9 \pm 0.1$ (Diemand et al. 2008, Springel et al. 2008). Remarkably, the normalized distribution of substructure depends very little on the overall scale of the halo, therefore we would expect approximately the same abundance of satellites around clusters and galaxies.

Although realistic simulations including baryons and non-gravitational effects have yet to be performed at this scale, it is currently believed that the statistical properties of the substructure inferred from N-body simulations should be robust enough to allow for a direct comparison with observations (see, e.g., Kravtsov 2010, and references therein). For these reasons such a comparison may provide one of the most stringent and direct tests of the CDM paradigm at subgalactic scales.

At variance with the results of simulations, the abundance of luminous satellites observed around real clusters and galaxies are very different. Whereas clusters of galaxies host thousand of galaxies within their own DM halos, fewer satellites

are generally seen around galaxies. In particular, the mass function of the luminous satellites of the Milky Way differs dramatically from that of the subhalos of a typical simulated halo of comparable mass. At the high mass end of the distribution (virial $M_{\text{sub}} \sim 10^9 M_{\odot}$) the observed number of satellites is comparable, or perhaps even slightly larger, than expected. However, the mass function of the halos of the observed satellites is found to be much shallower than that predicted for subhalos, resulting in a dramatic shortfall at lower masses, below $10^8 M_{\odot}$. This discrepancy between theory and observations has been known for over a decade (Klypin et al. 1999, Moore et al. 1999), and has not been solved by the revolutionary discovery of low luminosity satellites of the Milky Way by SDSS, nor by advances in numerical simulations. An up-to-date summary of the current state of the problem is given by Kravtsov (2010).

5.2 Possible solutions

There are two classes of possible explanations for the so-called “excess sub-halos problem” (or “missing satellites problem” if you are a theorist). One possible explanation is that substructure exists, but it is dark, i.e. subhalos do not form enough stars to be detected. This explanation would imply that the conversion of baryons into stars is inefficient for small halos. It is hard to explain this inefficiency with the known mechanisms of supernovae feedback or the effect of the UV ionizing background (Kravtsov 2010). Alternatively, it is possible that subhalos are not as abundant as predicted by numerical simulations. This explanation would imply a major revision of the standard CDM paradigm, either reducing the amplitude of fluctuations on the scales of satellites, or changing the nature of DM from cold to warm (Miranda & Macciò 2007). Either explanation

has far reaching implications. In order to be viable, the first explanation requires a clear improvement in our understanding of galaxy formation. In its most extreme version, the second explanation may require a re-thinking of the paradigm.

Gravitational lensing provides a unique insight into this problem, since it is arguably the only way to detect dark substructure, measure its mass function, and compare it with the prediction of CDM numerical simulations. Even if advances in theories of galaxy formation could explain the luminosity function of Milky Way satellites, there would still be a robust and falsifiable prediction of large numbers of darker satellites to be tested.

If the mass function of sub-halos turns out to be different than that predicted by simulations a major revision of the theory would be required, possibly requiring warm DM, although it is not clear that that would necessarily be compatible with all other constraints (see Kravtsov 2010, and references therein).

5.3 Flux ratio anomalies

The most striking and easiest to detect lensing effect of substructure is the perturbation of the magnification pattern. Since magnification depends on the second derivative of the potential, a small local perturbation can introduce dramatic differences in the observed surface brightness of the lensed source, without altering significantly the overall geometry of the system. For point sources, the presence of substructure results in ratios of the fluxes of multiple images that are significantly different than what would be predicted by a smooth macro model. This effect is often referred to as the anomalous flux ratios phenomenon, and has been used to infer the presence of substructure in lens galaxies (Bradač et al. 2002, Chiba 2002, Dalal & Kochanek 2002, Mao & Schneider 1998, Metcalf & Zhao 2002).

In an influential paper, Dalal & Kochanek (2002) analyzed radio data for a sample of seven quadruply imaged sources, and reported the detection of a surface mass fraction in the form of substructure between 0.6% and 7%. This observed fraction appears to be even higher than the mass fraction in substructure at the Einstein radius predicted by simulations (Mao et al. 2004, Xu et al. 2009).

Substantial efforts have been devoted to investigate whether satellite-size halos are the most likely explanation of the observed flux ratio anomalies. Indeed, flux ratio anomalies could also arise from other effects such as microlensing – if the source is sufficiently compact – or a non-uniform interstellar medium which could variously affect light propagating along different paths. However, both contaminants are wavelength dependent, while flux ratio anomalies due to the substructure are achromatic. Therefore, observations at multiple wavelengths, especially radio, narrow emission lines, and mid-infrared, can be used to show that the anomalous flux ratios are effectively due to substructures on scales much larger than stars (e.g., Agol, Jones & Blaes 2000; Kochanek & Dalal 2004; Moustakas & Metcalf 2003). Angular structure in the macro model has been suggested as a possible cause for flux ratio anomalies (Evans & Witt 2003). However, in the cases when enough azimuthal information is available it has been shown that the angular structure of lens galaxies is fairly simple and well approximated by an ellipse (Yoo et al. 2006). Elegant arguments based on the local curvature of the time-delay surface near the multiple images have also been used to show that anomalous flux ratios are indeed due to mass substructure (Chen 2009, Kochanek & Dalal 2004). A final source of concern is potential contamination from substructure along the line of sight, which could mimic the effects of true galactic satellites (Chen 2009; Chen, Kravtsov & Keeton 2003). Line-of-

sight contamination is most likely not the main cause of the anomalies observed so far. However, it is clear that line-of-sight contamination needs to be better understood and quantified in order to extract the maximum amount of information from this powerful tool.

An important question is whether the detected substructure is dark or luminous. In some cases (e.g. Koopmans et al. 2002; MacLeod, Kochanek & Agol 2009; McKean et al. 2007) it has been shown that mass associated with luminous satellites can explain the observed anomalies. Whether luminous substructure can explain all the known anomalies is still a matter of debate (Chen 2009). On a case by case basis, the role of luminous satellites is difficult to quantify because they are hard to detect in the vicinity of the bright lensed quasars, where they would be most effective in introducing anomalies. In addition to high resolution HST or adaptive optics images, an accurate determination of the luminosity function and spatial distribution of luminous satellites of (non-lensing) massive galaxies may be a way to make progress. The challenge is to collect large enough samples of non-lenses while carefully matching the selection process of the sample of lenses. It is important to stress that the detection of optical counterparts does not undermine the quest for substructure using gravitational lensing. Measuring the mass function of satellites - whether they are visible or not - is essential to test the CDM paradigm. Comparing the satellite mass function with their luminosity function will only help in answering some of the questions related to the mechanisms which regulate star formation.

The detection of substructure via anomalous flux ratios is an example of the power of gravitational lensing in measuring the distribution of mass in the universe. However, the strong lensing studies to date suffer from two fundamental

limitations, which need to be overcome in order to make progress. The first limitation is poor and uncertain statistics. Not only is the number of systems that can be used to study anomalous flux ratios tiny, but the selection function is poorly characterized. Therefore, the uncertainties are large and the results could be biased. The second major limitation is the limited mass sensitivity achieved so far, which is only sufficient to probe the upper end of the mass function of subhalos.

Major improvements on both aspects are underway and significant progress is possible in the next few years. One key factor is the increase in the number of known lenses, discovered with a well defined selection algorithm, coupled with the increased capability for follow-up. In the next decade, we may expect tens of thousands of lenses to be discovered by radio and optical surveys (§ 9). The other key factor is the development of advanced techniques to be applied to high resolution data to probe further down the mass function of subhalos, discussed next.

5.4 Astrometric and time-delay anomalies

Flux ratio anomalies is only one way to detect substructure. Subhalos affect all lensing observables, including deflection angles and time delays, and can therefore be detected as corresponding perturbations with respect to the predictions of a smooth model. Although these are more subtle effects, they have been shown to be sufficiently large to be used to detect substructure (e.g. Chen et al. 2007, Keeton & Moustakas 2009). Galaxy-galaxy lenses where the multiple images form an almost complete Einstein ring and are observed with high signal-to-noise ratio can detect individual substructures with masses as low as $\sim 10^8 M_\odot$

(Koopmans 2005, Vegetti & Koopmans 2009a). Recent calculations by Vegetti & Koopmans (2009b) indicate that current samples of galaxy-galaxy lens systems such as SLACS can detect subhalo mass fractions as low as 0.5%, assuming the slope of the mass function is well known from simulations. A sample of 200 Einstein rings with data of comparable quality to HST should be sufficient to start constraining the slope of the mass function as well. The sensitivity will be further enhanced with advances in resolution expected from future radio telescopes and the next generation of adaptive optics systems on large and extremely large telescopes. Furthermore, anomalous flux ratios, astrometric perturbations, and time delay anomalies depend on different moments of the satellite mass function (Keeton 2009). Therefore, a combination of techniques can help constrain both the slope and the normalization of the substructure mass function.

6 Cosmography

Cosmography is the measurement of the parameters that characterize the geometry, content, and kinematics of the universe. Much progress has been achieved in recent years (e.g., Komatsu et al. 2009), heralded as the era of precision cosmology. However, some of the fundamental parameters need to be measured even more accurately if one wants to discriminate between competing theories. For example, the equation of state of dark energy w and its evolution with cosmic time are essential ingredients to understand the nature of this mysterious phenomenon.

Strong lensing is a powerful cosmographic probe, as it depends on cosmological parameters in two ways. Firstly, the time delay equation (and the lens equation) contain ratios of angular diameter distances. Therefore, within the context of a

model for the lensing potential, measurements of time delays or mass act as standard rods, in a similar manner as the acoustic peaks of the power spectrum of the cosmic microwave background. Cosmography based on this concept is described in Sections 6.1, 6.2, and 6.3. Secondly, the optical depth for strong lensing depends on the number and redshift distribution of deflectors and therefore on the growth of structure and on the relation between redshift and comoving volume. Thus, given a model for the lensing cross section, and a model for the evolution of the population of deflectors, one can do cosmography from lens statistics. This approach is described in § 6.4.

6.1 Time delays

Consider a galaxy lensing a time-variable source like a quasar or a supernova. Under the thin lens approximation, multiple images will be observed to vary with a delay which depends on the gravitational potential as well on a ratio of angular diameter distances (Equation 1). The ratio of angular diameter distances is mostly sensitive to the Hubble Constant H_0 (hereafter h in units of $100 \text{ km s}^{-1} \text{ Mpc}^{-1}$). However, time delays also contain non-negligible information about other cosmological parameters, especially if one considers a sample of deflectors and sources spanning a range of redshifts (e.g. Coe & Moustakas 2009). Therefore, although it is convenient to think in terms of the Hubble constant as the primary parameter, time-delays provide constraints in the multidimensional cosmological parameter space. When combined with other cosmology probes like the CMB power spectrum, time-delays are very effective at breaking degeneracies such as that between H_0 and w (Figure 13).

From a practical point of view, cosmography with time-delays can be broken

into two separate problems: measuring time delays and modeling the lensing potential, including matter along the line of sight. Uncertainties in these two terms dominate the error budget and they are independent. Therefore, in order to measure H_0 to 1% accuracy from one lens system one needs to know both quantities with sub percent accuracy. Or, for a sample of N lenses, one needs unbiased measurements with approximately half $\sqrt{N}\%$ uncertainty on both quantities.

6.1.1 MEASURING TIME DELAYS Measuring time delays requires properly sampled light curves of duration significantly longer than the time-delay between multiple images. Once an approximate time-delay is known, the measurement can generally be refined by adapting the monitoring strategy, e.g. with dense sampling triggered after an event on the leading image. Typical time delays for galaxy lens systems are in the range weeks to months (with tails on both ends out to hours to years) and minimum detectable amplitudes from the ground are of order $\sim 5\%$, limited by photometric accuracy for crowded sources and microlensing (see § 7.3). Thus, accurate time-delays typically require several seasons of dedicated monitoring effort.

After the first “heroic” campaigns of the nineties and early 2000 (see Schneider, Kochanek & Wambsganss 2006, for a review), which yielded of order 10 time-delays, several groups are now trying to take this effort to the next level with the help of queue mode scheduling and robotic telescopes. A recent summary of published time-delay measurements is given by Jackson (2007). Two new time-delays have been published since then (J1206+4332 and J2033-4723; Paraficz, Hjorth & Elíasdóttir 2009; Vuissoz et al. 2008). Taking the published time-delay uncertainties at face value, the present sample contributes to the error budget on H_0 a little less than 1%. As I will discuss in § 9, time-domain astronomy is a rapidly growing field and it is likely that many

of the logistical problems faced by time-delay hunters so far will be solved in the next decade.

6.1.2 DETERMINATION OF THE LENSING POTENTIAL We now turn to errors associated with the local lensing potential, under the single screen approximation (matter along the line of sight and associated uncertainties will be described in § 6.1.3). At fixed image configuration, time-delays depend to first order on the effective slope of the mass distribution in the annular region between the multiple-images (see Saha & Williams 2006; Schneider, Kochanek & Wambsganss 2006, and references therein for discussion). For generic power-law models, at fixed lensing observables, the inferred H_0 scales as $H_0(\gamma') \approx (\gamma' - 1)H_0(\gamma' = 2)$. For many systems, especially doubly imaged point sources, the lensing potential is highly uncertain and dominates the error budget. Unaccounted uncertainties in the mass model are the main culprits for the reported discrepancies between time-delay determinations of H_0 as large as $\sim 30\%$ (e.g. Treu & Koopmans 2002b).

It is clear that some additional information is needed to bring the error budget on the lens modeling in line with that from time-delays. One approach consists of asserting some prior knowledge of the mass distribution in the deflectors and applying it to the analysis of a sample of systems. Since the effective slope is poorly constrained by lens data for point-like sources without additional information, the results depend critically on the prior. Following this approach, Oguri (2007) modeled 16 systems with power-law models assuming a Gaussian prior on γ' centered on 2 and width 0.15 obtaining $h = 0.68 \pm 0.06 \pm 0.08$ (the large systematic error attempts to reflect the large dispersion from system to system; however, it may also be due to the inclusion of systems with questionable redshift, time-delay or embedded in a complex cluster potential, which carries

substantial additional modelling uncertainties). The prior on γ is plausible but not strictly justified, since there are no independent measurements for the sample. For example, just changing the mean of the prior to $\langle\gamma'\rangle = 2.085^{+0.025}_{-0.018} \pm 0.1$ as found for the SLACS sample, would increase the estimate of H_0 by 8%, with an additional systematic uncertainty of 10%. A very similar approach is that by Coles (2008), who imposes geometric priors to his pixelized mass reconstructions and obtains $h = 0.71^{+0.06}_{-0.08}$ from 11 systems. Although it would be useful to draw samples from the Coles (2008) prior and measure the effective distribution of γ' , it appears that his smoothness and steepness constraints create a distribution of effective slopes similar to that of Oguri (2007), explaining the agreement. These results are encouraging. However, they illustrate the challenge of reaching 1% accuracy using this methodology. One needs to have sufficient external knowledge of the distribution of mass in the sample of galaxies with measured time-delays to construct a sufficiently accurate prior.

A more promising approach is to extract additional information for the very systems with measured time delays using ancillary data in addition to those available for the multiply-imaged point sources. In Bayesian terms, this means making the likelihood more constraining so as to reduce the relative importance of the prior. Following this approach, Wucknitz, Biggs & Browne (2004) modeled the extended radio structure around the lensed quasar in B0218+357 to infer $\gamma' = 1.96 \pm 0.02$ and $h = 0.78 \pm 0.03$. Koopmans et al. (2003b) modeled B1608+656 using the measured stellar velocity dispersion and the HST images of the lensed host galaxy to measure γ' and infer $h = 0.75^{+0.07}_{-0.06} \pm 0.03$, fixing $\Omega_m = 0.3$ and $\Omega_\Lambda = 0.7$, and neglecting uncertainties due to the mass-sheet degeneracy, discussed in the next section. A recent analysis of improved Keck

and HST data of B1608+656 by Suyu et al. (2010) using more general pixellated models for the potential and the source, infers $h = 0.706 \pm 0.031$, for the same cosmology as Koopmans et al. (2003b), including uncertainties related to the mass-sheet degeneracy. This results shows that modeling errors can be reduced to a few percent per lens system, if sufficient observational constraints are available. If the other cosmological parameters are allowed to vary, one obtains the constraints shown in Figure 13. The information from time delays is particularly powerful when combined to the WMAP5 results (Komatsu et al. 2009), improving from $h = 0.74^{+0.15}_{-0.14}$ and $w = -1.06^{+0.41}_{-0.42}$ to $h = 0.697^{+0.049}_{-0.05}$ and $w = -0.94^{+0.17}_{-0.19}$, for a flat cosmology. The results from a single lens are comparable with those from the local distance ladder method ($h = 0.742 \pm 0.036$ and $w = -1.12 \pm 0.12$ in combination with WMAP5; Riess et al. 2009) in terms of precision, although they are based on completely different physics and assumptions, and subject to different systematic errors.

6.1.3 MASS ALONG THE LINE OF SIGHT AND THE MASS-SHEET DEGENERACY

The final and perhaps limiting factor at this point is the uncertainty due to the unknown distribution of mass along the line of sight, i.e. deviations from the single screen approximation. On the one hand massive galaxies are typically found in groups. Group members and the common group halo contribute additional shear and convergence at the location of the main deflector. On the other hand, the “cone” between us the observer and source may be over or underdense, thus perturbing the time-delays with respect to those expected in a perfectly smooth and isotropic universe. Both effects can be thought to first order as equivalent to adding an external convergence κ_{ext} at the location of the deflector (which can be negative if the line of sight is underdense).

Due to the mass-sheet degeneracy, κ_{ext} is undetectable from dimensionless lensing observables. However, if we ignored its presence and make the standard assumption of vanishing convergence away from the lens to break the mass-sheet degeneracy, we would infer a biased value of H_0 by a factor $1/(1 - \kappa_{\text{ext}})$ (e.g. Schneider, Kochanek & Wambsganss 2006).

Independent measurements of mass, such as stellar velocity dispersion, help break the degeneracy because they constrain the local mass distribution. An unknown κ_{ext} leads to an overestimate of the lensing mass, and therefore alters the inferred γ' from comparison with kinematics, counterbalancing the effects on H_0 , but not exactly. Measurements of the local environment (e.g., Auger et al. 2007, Fassnacht et al. 2006, Momcheva et al. 2006) also help, although the limiting factor is the precision with which mass can be associated with visible tracers. A third approach consists of inferring the distribution of effective κ_{ext} from high resolution numerical simulations (Hilbert et al. 2007). The challenges of this third approach are producing realistic simulations at kpc scales relevant for strong lensing and understanding the selection function of the observed samples well enough to select simulated samples in the same way. In the case of B1608+656, the total uncertainty can be brought to 5% using a combination of the three approaches (Suyu et al. 2010). Analyzing a number of systems in similar detail will help uncover whether there are any residual significant biases.

6.2 Lenses as standard masses

Lensing studies indicate that the ratio f_{SIE} between stellar velocity dispersion measured within a standard spectroscopic aperture and the normalization of the best fit SIE model σ_{SIE} is close to unity (1.019 ± 0.08 for the SLACS sam-

ple for a concordance cosmology Bolton et al. 2008b), consistent with our general understanding of the mass distribution of early-type galaxies in the local Universe. If f_{SIE} is known sufficiently well – independent of cosmology – lens galaxies could effectively be used as standard masses plugging measurements of Einstein radius and stellar velocity dispersion into the SIE version of Eq. 9 (Grillo, Lombardi & Bertin 2008). Note that H_0 cancels out in the ratio of angular diameter distances. Unfortunately, our current understanding of the mass-structure of deflectors and of the distribution of matter along the line of sight is not sufficient for accurate cosmography (Schwab, Bolton & Rappaport 2010). In some sense, the situation is similar to that of time-delay cosmography, and similar methodologies could be applied to overcome the limitations. The advantage of this method over time-delays is that it can be applied to any lens regardless of the presence of a variable source. The disadvantage is that the sensitivity of the angular diameter distance ratio on cosmological parameters is weak.

6.3 Compound lenses

The Einstein radius of a gravitational lens depends on the mass enclosed and on ratios of angular diameter distances. For systems with multiple sets of multiple images, such as SDSSJ0946+1006 (Figure 10), one can solve for both the mass distribution and cosmography, provided that enough information is available to constrain the distribution of mass in the region between the Einstein rings. An additional complication is given by the mass associated with the inner ring, which acts as an extra deflector, making these systems compound lenses for the background source responsible for the outer ring. Gavazzi et al. (2008) calculate that a sample of 50 systems like SDSSJ0946+1006 – expected for future large lens

surveys – should constrain the equation of state of dark energy w to about 10% precision. As in the cases discussed above, the issue is whether systematics associated with modeling the deflector itself or the structure along the line of sight can be controlled with sufficient accuracy. High quality spatially resolved kinematic information should help constrain the mass model of the main foreground deflector and of the inner ring.

6.4 Lens statistics

For a given source population, the fraction of strongly lensed systems (i.e. the optical depth) depends on the cross section of the deflectors and on the abundance of deflectors. Thus, measuring the abundance of strongly lensed systems constrains the intervening cosmic volume. This is the essence of lens statistics as a tool for cosmography, although quantities such as the distribution of Einstein radii and source redshifts also contain cosmographic information. Note that lens-driven surveys are not nearly as sensitive as source-driven surveys (see Schneider, Kochanek & Wambsganss 2006, and references therein for a theoretical description).

The state of the art of this cosmographic application is the analysis of 11 CLASS and 16 SQLS samples (Chae 2007, Oguri et al. 2008), which yield rather weak bounds on cosmological parameters (e.g., $w = -1.1 \pm 0.6^{+0.3}_{-0.5}$ Oguri et al. 2008). Even though precision can certainly be improved by increasing sample size, the ultimate limit is set by systematic uncertainties. Accurate cosmography from strong lensing statistics requires accurate knowledge of: i) the mass-structure and shape of deflectors to compute cross-sections; ii) the contribution to the cross-section from large scale structures; iii) the number density of deflectors; iv)

the source luminosity function; v) the survey selection function. Quantities i to iv need to be known as a function of redshift. In conclusion, lens statistics poses three additional challenges (iii-v) over those in common with other cosmographic applications.

6.5 Is lensing competitive?

The studies mentioned in this section show that cosmography with strong-lensing gives results in agreement with independent probes, reinforcing the so-called concordance cosmology. However, the ultimate test for a method is when it breaks new ground in terms of precision, and the result is then confirmed independently. In my view, time-delays are the cosmographic application that stands the best chance of doing this for three reasons. First, two out of three major problems (time delay measurement and local mass model) have been solved and progress on the third (external convergence) is being made. Secondly, the inferred constraints are well suited to break degeneracies inherent to other methods such as the CMB power spectrum. Thirdly, time-delays can be measured for a number of lenses using relatively small ground based telescopes or will come for free from future synoptic telescopes. Fourthly, the method is completely independent of the local distance ladder method and therefore provides a valuable independent test on its systematic uncertainties (like calibration and metallicity dependency of the cepheid-luminosity relation). Lenses as standard masses and compound lenses seem to be valuable cosmographic tools if they can be applied efficiently with limited observational resources, perhaps “piggy-backing” on other studies (§ 9).

What is certainly very exciting and unique is the “inverse” application of cos-

mographic applications: learn about galaxy structure and evolution, on the basis of accurate cosmography from other probes. As mentioned in § 4, time-delays, the combination of lensing and dynamics, and compound lenses have all been demonstrated to provide unique insights into the structure of distant galaxies, which cannot be obtained in any other way. This is also true for lens statistics, which can be used to determine the growth of the galaxy mass function in a unique way, once the mass structure of each galaxy is understood from the other means discussed above (Chae 2007, Mitchell et al. 2005).

7 Lenses as Cosmic Telescopes

In a typical galaxy-scale strong lens system, the background source is magnified by an order of magnitude. Exploiting this effect, lensed galaxies at intermediate and high redshift can be studied with the same level of detail as non-lensed galaxies in the local universe (§ 7.1). Furthermore, the host galaxies of bright active galactic nuclei are “stretched away” from the wings of the point spread function, enabling precise measurements of their luminosity and size, and ultimately of the cosmic evolution of the relation between host galaxy and central black hole (§ 7.2). Finally, microlensing by stars provides us with unique spatial information on the scale of the accretion disk, which is orders of magnitudes smaller than anything that can be resolved from the ground at any wavelength (§ 7.3).

7.1 Small and faint galaxies

The resolution of HST and the sensitivity of radio interferometers mean that we know very little about the distant ($z \gg 0.1$) universe on scales below ~ 1 kpc. Indeed, even in the nearby universe ($z \sim 0.1$), large ground based surveys

such as SDSS do not provide much sub-kpc scale information. Yet, we know from the local volume that small and faint galaxies are an essential ingredient of the universe, acting as building blocks of more massive systems. Only with the aid of gravitational lensing we can resolve sub-kpc scales and determine the morphology and size (Marshall et al. 2007), and kinematics of small galaxies as well as trace the location of star formation and the pattern of chemical abundances (Riechers et al. 2008, Stark et al. 2008). Furthermore, flux magnification enables detailed spectroscopic studies that would be prohibitive in the absence of lensing (Stark et al. 2008). These pilot studies show that intrinsic properties can be robustly recovered via lens modeling. The rapid increase in the number of known lenses should soon provide the large statistical samples needed for high impact studies.

7.2 Host galaxies of lensed active nuclei

In the local universe, massive galaxies are found to harbor central supermassive black holes. Remarkably, the mass of the black hole correlates with kpc-scale properties of the host bulge, such as velocity dispersion, luminosity and stellar mass (e.g. Gültekin et al. 2009). This family of correlations has been interpreted as evidence that black hole growth and energy feedback from active galactic nuclei play an important role in galaxy formation and evolution (e.g. Hopkins, Murray & Thompson 2009). However, the physics of the interaction as well as the relative timing of galaxy formation and black hole growth are poorly understood. Although the local relations are an important constraint, observing their cosmic evolution is necessary to answer some fundamental questions. Are the local relations only the end-point of evolution, or are they established

early-on? Which comes first, the black hole or the host bulge?

It is challenging to answer these questions observationally. Direct dynamical black hole mass measurements can only be done in the very local universe. At intermediate and high- z redshift, one needs to rely on indirect methods such as the empirically calibrated relation with continuum luminosity and line width observed for type-1 active galactic nuclei (AGN). However, the presence of bright luminous point sources hampers the study of the host galaxy (Jahnke et al. 2009, Treu et al. 2007). Strong lensing helps by stretching the host galaxy of distant lensed quasars primarily along the tangential direction (Figure 14). Of course, the quasar is also magnified, but one generally wins because the surface brightness of the point spread function falls off more rapidly than linearly. Using this method, Peng et al. (2006) showed that the bulges of host galaxies of distant quasars are more luminous than expected based on the local relation, consistent with a scenario where bulge formation predates black hole growth, at least for some objects. Similar results have been found for non-lensed AGN (Treu et al. 2007). However, without the aid of lensing, studies have to be limited to lower redshifts and lower luminosity AGNs.

7.3 Structure of active galactic nuclei

Understanding the physics of accretion disks and the regions surrounding supermassive black holes is essential to explain the AGN phenomenon with all its implications for galaxy formation and evolution. However, the scales involved are extremely small by astronomical standards (for a typical $10^9 M_\odot$ black hole, the Schwarzschild radius is $\approx 3 \cdot 10^{14}$ cm, the broad line region is $\sim 10^{17-18}$ cm), and therefore impossible to resolve with conventional imaging techniques.

Microlensing is perhaps the only tool capable of probing the small scales of the accretion disk. The Einstein radius of a star of mass M_s (Fig. 4), corresponds to approximately $4 \cdot 10^{16} \sqrt{M_s/M_\odot} \text{ cm} \approx 0.01 \sqrt{M_s/M_\odot} \text{ pc}$ when projected at the redshift of a typical lensed quasar ($z_d = 0.5$; $z_s = 2$ Schneider, Kochanek & Wambsganss 2006). The inner parts of the accretion disk will be smaller than this scale and therefore subject to microlensing, while the broad line region and the outer dusty torus should be largely unaffected. The characteristic timescale for variation is given by the microlensing caustic crossing time, typically of order years, although it can be shorter for special redshift combinations such as that of Q2237+030 (Schneider, Kochanek & Wambsganss 2006).

Based on this principle, one can infer the characteristic size of the accretion disk as a function of wavelength. Long-light curves – where the gravitational time delay between multiple images can also be determined – provide the most stringent limits (Kochanek 2004), but interesting information can also be obtained from single epoch data on a statistical basis (e.g. Bate, Webster & Wyithe 2007; Pooley et al. 2009).

The inferred absolute size of the accretion disk can be known up to a factor of order unity, which depends on $\langle M_s \rangle$ and on the relative transverse speeds between the stars, the deflector, and the source. However, the slope of the relation between accretion disk temperature and size is independent of that factor and can thus be determined more precisely. Current results indicate that the accretion disk is approximately the size expected for Shakura & Sunyaev (1973) disks, although discrepancies of order a factor of a few have been reported (Pooley et al. 2007). Assuming that the size scales as $\lambda^{1/\eta}$, η is found to be in the range 0.5–1, whereas $\eta = 0.75$ is expected for a Shakura & Sunyaev (1973) disk (Eigenbrod et al. 2008;

Poindexter, Morgan & Kochanek 2008). Long wavelength data imply the presence of a second spectral component, consistent with the hypothesis of a dusty torus of size much larger than the microlensing scale (Agol et al. 2009).

These first exciting results are just the beginning, because very few light curves obtained so far are long enough to harness the full power of microlensing. With the rapid development of time-domain astronomy predicted for the next decade, multiwavelength monitoring campaigns of several years for tens of objects should become feasible (§ 9).

7.4 Cosmic telescopes and human telescopes

I have described how strong lensing provides a unique opportunity to study sources that are too faint or too small to be studied otherwise, from quasar host galaxies to microarcsecond size accretion disks.

Unfortunately, the use of galaxies (and clusters) as cosmic telescopes is often more contentious than it should be. One frequent critique is that source reconstruction is difficult and inherently uncertain. This is a false perception. The brief discussion in § 2 and the references listed therein provide ample documentation that lens modeling is now a mature field with very well understood uncertainties, capable of delivering results that are well reproduced by independent analyses. Lens modeling at cluster scales is more complex due to the larger dynamic range in the data and the more inhomogeneous mass distribution. Nevertheless, robust results can be obtained also for clusters, provided that enough information is available.

Another frequent critique is that surveys using cosmic telescopes are inefficient compared to blank fields because of magnification bias. This is true for sources

with number counts in flux units (dN/dF) flatter than F^{-1} . However, when probing the bright-end of the luminosity function of any population – where number density falls off exponentially – lensing is just unbeatable: the brighter of any class of distant astronomical objects will inevitably be gravitationally lensed. Cosmic telescopes and blank surveys are complementary to fully characterize a source population and its physical properties.

8 Searches for Gravitational Lenses

The strong lensing applications covered in this article span a broad range of astrophysical phenomena, observational, and theoretical challenges. However, they all share a common limitation: the relatively small number of systems to which they can be applied. Although there are 200 systems known, they are not all suitable for all applications. Studies must rely on at most a few tens of cases to infer results of general interest.

Fortunately, a number of large surveys are expected to take place in the next decade, providing an ideal dataset to mine for rare objects such as strong lenses. The challenge will consist in developing fast and robust algorithms to find new lenses, and then in mustering the resources and the brain power needed to follow them up and study them (§ 9).

Before I summarize some of the searching techniques, it is useful to establish a discovery “etiquette”: what are the necessary and sufficient elements to identify a strong gravitational lens? Here are two necessary criteria: i) multiple images clearly identified; ii) image configuration reproduced by a “simple” model. The first criterion seems to me unavoidable, although it has not always been applied in the past. The second criterion is more subjective, but can be made quantitative

in the following way. Given our knowledge of the surface brightness distribution of galaxies and of the gravitational potential, is it more likely that the observed configuration arises from some random configuration (e.g., HII regions distributed along a cross-pattern, or two quasars with similar colors on the opposite sides of a galaxy), or from strong lensing of a more common surface brightness distribution? It seems to me these two criteria are also sufficient. Additional criteria such as images having identical colors or spectroscopic redshift of deflector and source are desirable, but impractical for future surveys that may have high resolution images in just a single band, or limited capabilities for spectroscopic follow-up.

8.1 Imaging-based searches

Imaging-based searches can be divided into catalog-based and pixel-based. Catalog-based searches look for objects in a lensing-like configuration. They are most effective at detecting sharp multiply-imaged features such as multiply-imaged quasars (e.g. Inada et al. 2008, Oguri et al. 2008), but they can also be used for extended sources, provided the image separation is large enough for deblending (Allam et al. 2007, Belokurov et al. 2007). Pixel-based searches start from a set of pixels, and look for lensing-like configurations. Lenses are identified on the basis of characteristic geometries (e.g. Cabanac et al. 2007) or by actually modeling every system as a possible lens (Marshall et al. 2009). The pixel-based method is slower and more computationally intensive than catalog-based searches, but in principle can be used to push the detection limit to smaller angular separations, beyond the level where source and deflector can be deblended by general-purpose cataloging softwares. Visual searches can be considered as pixel-based, with the human brain as lens-modeling tool (e.g.

Jackson 2008; Newton, Marshall & Treu 2009). Algorithms need to be tweaked to reach an optimal balance between completeness (false negative) and purity (false positive) appropriate for each dataset and scientific goal. The best algorithms can currently achieve 90% completeness and purity searching through HST data (Marshall et al. 2009; Newton, Marshall & Treu 2009). Although some human intervention is still necessary, this breakthrough makes it feasible to search through future surveys of 1000 deg² or more.

Time-domain surveys allow for a different image-based strategy: looking for variable resolved sources (Kochanek et al. 2006a). At high galactic latitude, lensed quasars are more common than contaminants such as pairs of variable stars. Pairs of non-lensed quasars can be distinguished on the basis of their light curves and colors, while lensed supernovae are a welcome contaminant (see § 9). A first application of the method to the SDSS Supernovae survey data show that the only known compelling lens candidate is recovered as a close pair of variable sources. Out of over 20,000 sources, only a handful of false positives are found, suggesting a “purity” of $\sim 20\%$ (Lacki et al. 2009). This is encouraging, although more tests on wider and deeper data are needed to further improve the method in view of upcoming surveys.

8.2 Spectroscopy-based searches

Spectroscopic searches rely on identifying composite spectra with features coming from multiple redshifts. Follow-up high resolution information is then needed to identify the subset of events with detectable multiple-images, and to obtain astrometry for lens modeling. A strong advantage of the method is that lenses come with redshifts by construction. After the early serendipitous discoveries

(Huchra et al. 1985), the method started to bear large numbers of lenses only with the SDSS spectroscopic database (Auger et al. 2009, Bolton et al. 2008a, 2006, Willis et al. 2006). The recent searches highlight the quality of spectroscopic data as the key element for success. High signal-to-noise ratios are needed to identify faint spectral features, close-to Poisson limited sky subtraction is needed to reduce false positives, spectral resolution better than 100 km s^{-1} is needed to resolve line multiplets, and wide wavelength coverage increases the redshift range for the search. It is a testament to the high quality of the SDSS database that the confirmation rate is $\sim 60 - 70 \%$ (Bolton et al. 2008a), after a very strict initial selection (approximately 1/1000 SDSS galaxies are selected as a candidate for follow-up by SLACS).

9 Future Outlook

9.1 Thousands of gravitational lenses

Most of the applications listed in the previous sections are listed by sample size. An increase by one of order of magnitude in sample size is needed to make progress. Fortunately, there is a realistic opportunity to make this happen in the next decade, considering the typical yields for strong lens systems searches. For optical and near infrared imaging searches, yields are $\sim 10 \text{ deg}^{-2}$ at HST-like depth and resolution (Marshall, Blandford & Sako 2005), $\sim 1 \text{ deg}^{-2}$ at the best ground based conditions (Cabanac et al. 2007). At radio wavelengths and $0''.25$ resolution expected for the Square Kilometer Array (Koopmans et al. 2009a) the yield is $\sim 1 \text{ deg}^{-2}$. For spectroscopic surveys, the yield is $\sim 10^{-3}/\text{spectrum}$. Thus, a 1000 deg^2 HST-quality cosmic shear survey, all sky ground based surveys in the optical or radio, and a 10^7 galaxy redshift survey should all be capable of yielding

$\sim 10,000$ strong gravitational lens systems, although with different properties. High angular resolution surveys will be critical for applications such as the study of small mass deflectors and of the substructure mass function. Time-domain surveys will have a built-in advantage for, e.g., time-delays and microlensing. Spectroscopic surveys will be advantageous for those applications that require redshift and velocity dispersions, such as the study of luminous and dark matter in the deflector. Several thousand strong lens systems from each of these search techniques is an ambitious, yet feasible, goal for the next decade.

These massive undertakings will require large number of people and resources. As in many other instances, it is likely that such projects will require the joint efforts of a number of communities interested in diverse scientific questions. The unique capabilities of strong lensing make it very worthwhile to design future surveys keeping in mind its requirements.

9.2 The problem of follow-up

Let us assume that 10,000 strong lens candidates have been found. What follow-up will be needed to extract scientific information? Images with resolution of order $0''.1$ are often key to prove the lensing hypothesis, and to construct detailed lens models and study the properties of the host and the source. If the resolution of the finder survey is not adequate, follow-up will be required. Current follow-up imaging typically requires an orbit of HST. JWST should gain in speed for most applications and be revolutionary for long-wavelength studies, such as flux ratio anomalies. For a subset of objects with suitable colors and nearby stars, high resolution imaging could perhaps also be obtained in a comparable amount of time with a 8-10m telescope equipped with laser guide star adaptive optics

(LGSAO). Extremely large 30-m class telescopes (ELTs) with LGSAO should be able to gain a substantial factor in speed and resolution. Radio follow-up of extended sources at high resolution with VLA requires of order 1 hour per lens. The Atacama Large Millimeter/Submillimeter Array (ALMA) should be an improvement both in speed and resolution. Even following up a thousand lenses will thus require thousands of hours of telescope time, maybe a few hundreds with JWST, ELTs and ALMA. This may be feasible, but not trivial, making high resolution imaging a likely bottle neck. Multiplexing is unlikely to be an option given the rarity of these objects on the sky, although multiplexing with different astronomical targets is certainly a desirable option. Even higher resolution images ($0''.01$) are within reach with extreme adaptive optics on extremely large telescopes and will certainly be beneficial for pushing some of the lensing applications. For example, that kind of resolution could push the detection of DM substructure in distant galaxies in the $10^7 M_\odot$ regime typical of the least massive luminous Milky Way satellites currently known, where the discrepancy with theory is currently strongest (Kravtsov 2010).

Spectroscopic follow-up to gather redshifts is a problem of possibly even greater magnitude, considering that redshifts for many of the sources cannot be measured even spending hours on the largest telescopes (Ofek et al. 2006). For the fainter sources, photometric redshifts may be the only option. Coordination with redshift surveys – such as those proposed to measure baryonic acoustic oscillations – will help measuring redshifts as well as in spectroscopic searches, although they will also require high angular resolution follow-up.

Monitoring campaigns of thousands of lensed AGNs are out of the question at the moment, but could be a natural byproduct of future synoptic surveys. Some

of the most demanding time domain applications, such as detection of time-delay anomalies could be beyond the reach of ground based monitoring tools and require a dedicated space mission (Moustakas et al. 2008).

In parallel with discovery efforts, careful thought must be put into planning follow-up efforts. First, ways to extract as much information as possible from the discovery images themselves must be found. Second, follow-up efforts should be coordinated as much as possible with those of other science cases to find common paths and synergies. Last but not least, brain power could be another serious limitation. Currently, accurate and reliable lens models require several days of expert human brain activity. This will not be possible when samples will consist of tens of thousands of systems.

9.3 Unusual lensing applications in an era of abundance

I conclude with four examples of strong lensing applications that require very rare conditions and therefore need the large samples expected in the next decade to become viable.

Lensed supernovae Ia are extremely valuable, because their standard luminosity constrains the absolute magnification and therefore breaks the mass-sheet degeneracy. For typical rates, we expect of order one could be found monitoring known lenses. However, a ground based time-domain survey covering most of the sky is expected to find of order a hundred lensed type Ias (Oguri & Marshall, 2009, in preparation).

Compound lenses are potentially powerful cosmographic probes, but there is currently only one such system known at galaxy scales (Gavazzi et al. 2008). Thousand square degree field surveys at HST-like resolution should be able to

find tens of systems like SDSSJ0946+1006, potentially constraining w to the 10 % level (Gavazzi et al. 2008).

Strong lensing is one of the few tools capable of measuring the mass of quiescent black holes at cosmological distances, through their gravity affects the properties of central images (Mao, Witt & Koopmans 2001). Detecting the central image – which is generally highly demagnified – is usually beyond reach with current instrumentation (see however Winn, Rusin & Kochanek 2004). However this application may become practical with future facilities, especially at radio wavelengths where the contrast between deflector and source is more favorable.

Finally, with future samples of 10^4 lenses, rare examples of “catastrophes” should be identifiable (Orban de Xivry & Marshall 2009). These are very special lensing configurations characterized by specific constraints on the gravitational potential and its derivatives, and they only occur only for very specific source position and redshift (see Petters, Levine & Wambsganss 2001; Schneider, Ehlers & Falco 1992, for details). The identification of examples of catastrophes is interesting for two reasons. Firstly, catastrophes often lead to extreme magnification factors, up to ~ 100 , making them extraordinary cosmic telescopes. Secondly, the unusual geometry of multiple images can give remarkably strong constraints on the mass distribution of the deflector (Orban de Xivry & Marshall 2009).

Acknowledgments

I am grateful to Matt Auger, Maruša Bradač, Brendon Brewer, Chris Fassnacht, Raphael Gavazzi, Leon Koopmans, Phil Marshall, Elisabeth Newton, Carlo Nipoti, Andrea Ruff, Anna Pancoast, and Sherry Suyu for helpful comments on early drafts of this article. I would like to thank in particular Richard El-

lis for his many insightful comments and advice about this article and throughout the past decade. I am also grateful to Roger Blandford, for his scientific input and feedback as editor. Finally, I would like to acknowledge enlightening conversations with many people including Giuseppe Bertin, Chris Kochanek, Jean-Paul Kneib, Paul Schechter, Peter Schneider, and Joachim Wambsganss. Financial support from the Sloan and Packard Foundations is gratefully acknowledged.

Acronyms

1. CDM: Cold Dark Matter
2. CMB: Cosmic Microwave Background
3. DM: Dark Matter
4. HST: Hubble Space Telescope
5. IMF: Initial Mass Function
6. JWST: James Webb Space Telescope
7. SDSS: Sloan Digital Sky Survey
8. SIE: Singular Isothermal Ellipsoid
9. SIS: Singular Isothermal Sphere
10. SLACS: Sloan Lens Advanced Camera (for Surveys) Survey

Definitions

1. Convergence: dimensionless projected surface mass density in units of the critical density.
2. Deflector: the foreground galaxy responsible for the lensing potential.

3. Einstein radius: characteristic scale of strong lensing. For a circular deflector it corresponds to the radius within which $\langle \kappa \rangle = 1$.
4. Image plane: twodimensional map of the source emission as it appears to the observer after propagation through the lensing potential.
5. Macrolensing: strong lensing producing image separations of order arcseconds, the typical scale of massive galaxies.
6. Microlensing: strong lensing producing image separation of order of microarcseconds, the typical scale of individual stars.
7. Millilensing: strong lensing producing image separation of order of milliarcseconds, the typical scale of small satellite galaxies.
8. Shear: dimensionless quantity that describes the local distortion of lensed images.
9. Source: the background astronomical object whose light is being lensed.
10. Source plane: twodimensional map of the source emission as it would appear to the observer in the absence of a deflector.
11. Strong lensing: deflection of light from a background source by a foreground deflector strong enough to produce multiple images.

Summary Points

1. Massive early-type galaxies are surrounded by dark matter halos spatially more extended than the luminous component. The fraction of mass in the form of dark matter inside the effective radius increases with galaxy stellar mass.

2. The total mass density profile of massive early-type galaxies is approximately isothermal in the innermost ~ 10 kpc, i.e. the logarithmic slope γ' equals two within 10%.
3. Precise gravitational time delays for a single system can be used to measure the Hubble Constant to 5% precision, provided that enough information is available to constrain the local gravitational potential and to break the mass-sheet degeneracy. Time delays break the degeneracy between h and w in the analysis of CMB data. Combining the constraints from the lens system B1608+656 and those from WMAP5 yields $h = 0.697^{+0.049}_{-0.050}$ and $w = -0.94^{+0.17}_{-0.19}$ assuming flatness.
4. The host galaxies of distant luminous quasars appear to be underluminous in comparison with local galaxies hosting black holes of the same mass. This may indicate that in this mass range black holes complete their growth before their host galaxy.
5. Microlensing results indicate that the size of accretion disks and its dependency on temperature is in broad agreement with the predictions of Shakura & Sunyaev (1973) models. Moreover, mid-infrared microlensing studies are consistent with a presence of an unresolved dusty region, larger than the accretion disk.

Future Issues

1. How do luminous and dark matter density profiles depend on galaxy mass, type, and cosmic time?
2. Are dark matter density profiles universal, as predicted by CDM numerical

simulations?

3. Is the mass function of substructure in agreement with the predictions of CDM numerical simulations?
4. How are density profiles and the substructure mass function influenced by the presence of baryons?
5. Is dark energy the cosmological constant ($w = -1$)? If not, how does the equation of state evolve with cosmic time?
6. How can we find and exploit larger samples of strong gravitational lens systems?

10 LITERATURE CITED

References

1. Agol E, Gogarten SM, Gorjian V, Kimball A. 2009. *ApJ* 697:1010–1019
2. Agol E, Jones B, Blaes O. 2000. *ApJ* 545:657–663
3. Allam SS, Tucker DL, Lin H, Diehl HT, Annis J, et al. 2007. *ApJL* 662:L51–L54
4. Auger MW, Fassnacht CD, Abrahamse AL, Lubin LM, Squires GK. 2007. *AJ* 134:668–679
5. Auger MW, Treu T, Bolton AS, Gavazzi R, Koopmans LVE, et al. 2009. *ApJ* 705:1099–1115
6. Barnabè M, Czoske O, Koopmans LVE, Treu T, Bolton AS, Gavazzi R. 2009. *MNRAS* 399:21–36
7. Bate NF, Webster RL, Wyithe JSB. 2007. *MNRAS* 381:1591–1596
8. Bell EF, de Jong RS. 2001. *ApJ* 550:212–229

9. Belokurov V, Evans NW, Moiseev A, King LJ, Hewett PC, et al. 2007. *ApJL* 671:L9–L12
10. Bertin G, Stiavelli M. 1993. *Reports on Progress in Physics* 56:493–556
11. Blandford RD, Narayan R. 1992. *ARA* 30:311–358
12. Bolton AS, Burles S, Koopmans LVE, Treu T, Gavazzi R, et al. 2008a. *ApJ* 682:964–984
13. Bolton AS, Burles S, Koopmans LVE, Treu T, Moustakas LA. 2006. *ApJ* 638:703–724
14. Bolton AS, Treu T, Koopmans LVE, Gavazzi R, Moustakas LA, et al. 2008b. *ApJ* 684:248–259
15. Bradač M, Schneider P, Steinmetz M, Lombardi M, King LJ, Porcas R. 2002. *A&A* 388:373–382
16. Brewer BJ, Lewis GF. 2006. *ApJ* 637:608–619
17. Browne IWA, et al. 2003. *MNRAS* 341:13–32
18. Bundy K, Treu T, Ellis RS. 2007. *ApJL* 665:L5–L8
19. Cabanac RA, Alard C, Dantel-Fort M, Fort B, Gavazzi R, et al. 2007. *A&A* 461:813–821
20. Cappellari M, Bacon R, Bureau M, Damen MC, Davies RL, et al. 2006. *MNRAS* 366:1126–1150
21. Chabrier G. 2003. *PASP* 115:763–795
22. Chae KH. 2007. *ApJL* 658:L71–L74
23. Chen J. 2009. *A&A* 498:49–60
24. Chen J, Kravtsov AV, Keeton CR. 2003. *ApJ* 592:24–31

25. Chen J, Rozo E, Dalal N, Taylor JE. 2007. *ApJ* 659:52–68
26. Chiba M. 2002. *ApJ* 565:17–23
27. Ciotti L, Lanzoni B, Renzini A. 1996. *MNRAS* 282:1–12
28. Coe D, Moustakas LA. 2009. *ApJ* 706:45–59
29. Coles J. 2008. *ApJ* 679:17–24
30. Courbin F, Saha P, Schechter PL. 2002 608:1–+
31. Courteau S, Rix HW. 1999. *ApJ* 513:561–571
32. Dalal N, Kochanek CS. 2002. *ApJ* 572:25–33
33. Diemand J, Kuhlen M, Madau P, Zemp M, Moore B, et al. 2008. *Nature* 454:735–738
34. Dutton AA, van den Bosch FC, Dekel A, Courteau S. 2007. *ApJ* 654:27–52
35. Dye S, Warren SJ. 2005. *ApJ* 623:31–41
36. Eigenbrod A, Courbin F, Sluse D, Meylan G, Agol E. 2008. *A&A* 480:647–661
37. Ellis R, Silk J. 2009. *to appear in "Structure Formation in the Universe", ed. Chabrier, Cambridge University Press*
38. Evans NW, Witt HJ. 2003. *MNRAS* 345:1351–1364
39. Falco EE. 2005. *New Journal of Physics* 7:200–+
40. Falco EE, Gorenstein MV, Shapiro II. 1985. *ApJL* 289:L1–L4
41. Fassnacht CD, Blandford RD, Cohen JG, Matthews K, Pearson TJ, et al. 1999. *AJ* 117:658–670
42. Fassnacht CD, Gal RR, Lubin LM, McKean JP, Squires GK, Readhead ACS. 2006. *ApJ* 642:30–38
43. Faure C, Kneib JP, Covone G, Tasca L, Leauthaud A, et al. 2008. *ApJS* 176:19–38

44. Féron C, Hjorth J, McKean JP, Samsing J. 2009. *ApJ* 696:1319–1338
45. Gavazzi R, Treu T, Koopmans LVE, Bolton AS, Moustakas LA, et al. 2008. *ApJ* 677:1046–1059
46. Gavazzi R, Treu T, Rhodes JD, Koopmans LVE, Bolton AS, et al. 2007. *ApJ* 667:176–190
47. Gerhard O, Kronawitter A, Saglia RP, Bender R. 2001. *AJ* 121:1936–1951
48. Grillo C, Gobat R, Lombardi M, Rosati P. 2009. *A&A* 501:461–474
49. Grillo C, Lombardi M, Bertin G. 2008. *A&A* 477:397–406
50. Gültekin K, Richstone DO, Gebhardt K, Lauer TR, Tremaine S, et al. 2009. *ApJ* 698:198–221
51. Hilbert S, White SDM, Hartlap J, Schneider P. 2007. *MNRAS* 382:121–132
52. Hoekstra H, Hsieh BC, Yee HKC, Lin H, Gladders MD. 2005. *ApJ* 635:73–85
53. Hopkins PF, Murray N, Thompson TA. 2009. *MNRAS* 398:303–311
54. Huchra J, Gorenstein M, Kent S, Shapiro I, Smith G, et al. 1985. *AJ* 90:691–696
55. Humphrey PJ, Buote DA, Gastaldello F, Zappacosta L, Bullock JS, et al. 2006. *ApJ* 646:899–918
56. Inada N, Oguri M, Becker RH, Shin MS, Richards GT, et al. 2008. *AJ* 135:496–511
57. Jackson N. 2007. *Living Reviews in Relativity* 10:4–+
58. Jackson N. 2008. *MNRAS* 389:1311–1318
59. Jahnke K, Bongiorno A, Brusa M, Capak P, Cappelluti N, et al. 2009. *ApJL* 706:L215–L220
60. Jiang G, Kochanek CS. 2007. *ApJ* 671:1568–1578

61. Keeton CR. 2009. *ArXiv e-prints*
62. Keeton CR, Gaudi BS, Petters AO. 2003. *ApJ* 598:138–161
63. Keeton CR, Moustakas LA. 2009. *ApJ* 699:1720–1731
64. Klypin A, Kravtsov AV, Valenzuela O, Prada F. 1999. *ApJ* 522:82–92
65. Kochanek CS. 1995. *ApJ* 445:559–577
66. Kochanek CS. 2004. *ApJ* 605:58–77
67. Kochanek CS, Dalal N. 2004. *ApJ* 610:69–79
68. Kochanek CS, Mochejska B, Morgan ND, Stanek KZ. 2006a. *ApJL* 637:L73–L76
69. Kochanek CS, Morgan ND, Falco EE, McLeod BA, Winn JN, et al. 2006b. *ApJ* 640:47–61
70. Kolatt TS, Bartelmann M. 1998. *MNRAS* 296:763–772
71. Komatsu E, Dunkley J, Nolte MR, Bennett CL, Gold B, et al. 2009. *ApJS* 180:330–376
72. Koopmans LVE. 2005. *MNRAS* 363:1136–1144
73. Koopmans LVE, Barnabe M, Bolton A, Bradac M, Ciotti L, et al. 2009a. *Astronomy* 2010:159–+
74. Koopmans LVE, Biggs A, Blandford RD, Browne IWA, Jackson NJ, et al. 2003a. *ApJ* 595:712–718
75. Koopmans LVE, Bolton A, Treu T, Czoske O, Auger MW, et al. 2009b. *ApJL* 703:L51–L54
76. Koopmans LVE, Garrett MA, Blandford RD, Lawrence CR, Patnaik AR, Porcas RW. 2002. *MNRAS* 334:39–47

77. Koopmans LVE, Treu T, Bolton AS, Burles S, Moustakas LA. 2006. *ApJ* 649:599–615
78. Koopmans LVE, Treu T, Fassnacht CD, Blandford RD, Surpi G. 2003b. *ApJ* 599:70–85
79. Kormann R, Schneider P, Bartelmann M. 1994. *A&A* 284:285–299
80. Kravtsov A. 2010. *Advances in Astronomy* 2010
81. Lacki BC, Kochanek CS, Stanek KZ, Inada N, Oguri M. 2009. *ApJ* 698:428–438
82. Lagattuta DJ, Fassnacht CD, Auger MW, Marshall PJ, Bradač M, et al. 2009. *ApJ* submitted
83. MacLeod CL, Kochanek CS, Agol E. 2009. *ApJ* 699:1578–1583
84. Maller AH, Flores RA, Primack JR. 1997. *ApJ* 486:681–+
85. Mandelbaum R, van de Ven G, Keeton CR. 2009. *MNRAS* :1066–+
86. Mao S, Jing Y, Ostriker JP, Weller J. 2004. *ApJL* 604:L5–L8
87. Mao S, Schneider P. 1998. *MNRAS* 295:587–+
88. Mao S, Witt HJ, Koopmans LVE. 2001. *MNRAS* 323:301–307
89. Marshall P. 2006. *MNRAS* 372:1289–1298
90. Marshall P, Blandford R, Sako M. 2005. *New Astronomy Review* 49:387–391
91. Marshall PJ, Hogg DW, Moustakas LA, Fassnacht CD, Bradač M, et al. 2009. *ApJ* 694:924–942
92. Marshall PJ, Treu T, Melbourne J, Gavazzi R, Bundy K, et al. 2007. *ApJ* 671:1196–1211
93. McKean JP, Koopmans LVE, Flack CE, Fassnacht CD, Thompson D, et al. 2007. *MNRAS* 378:109–118

94. Metcalf RB, Zhao H. 2002. *ApJL* 567:L5–L8
95. Miranda M, Macciò AV. 2007. *MNRAS* 382:1225–1232
96. Mitchell JL, Keeton CR, Frieman JA, Sheth RK. 2005. *ApJ* 622:81–98
97. Momcheva I, Williams K, Keeton C, Zabludoff A. 2006. *ApJ* 641:169–189
98. Moore B, Ghigna S, Governato F, Lake G, Quinn T, et al. 1999. *ApJL* 524:L19–L22
99. Moustakas LA, Bolton AJ, Booth JT, Bullock JS, Cheng E, et al. 2008 7010
100. Moustakas LA, Metcalf RB. 2003. *MNRAS* 339:607–615
101. Moustakas LA, et al. 2007. *ApJL* 660:L31–L34
102. Navarro JF, Frenk CS, White SDM. 1997. *ApJ* 490:493–+
103. Newton ER, Marshall PJ, Treu T. 2009. *ApJ* 696:1125–1141
104. Nipoti C, Treu T, Bolton AS. 2009. *ApJ* 703:1531–1544
105. Ofek EO, Maoz D, Rix HW, Kochanek CS, Falco EE. 2006. *ApJ* 641:70–77
106. Oguri M. 2007. *New Journal of Physics* 9:442–+
107. Oguri M, Inada N, Pindor B, Strauss MA, Richards GT, et al. 2006. *AJ* 132:999–1013
108. Oguri M, Inada N, Strauss MA, Kochanek CS, Richards GT, et al. 2008. *AJ* 135:512–519
109. Orban de Xivry G, Marshall P. 2009. *MNRAS* 399:2–20
110. Paraficz D, Hjorth J, Elíasdóttir Á. 2009. *A&A* 499:395–408
111. Peng CY, Impey CD, Rix HW, Kochanek CS, Keeton CR, et al. 2006. *ApJ* 649:616–634
112. Petters AO, Levine H, Wambsganss J. 2001

- 113. Poindexter S, Morgan N, Kochanek CS. 2008. *ApJ* 673:34–38
- 114. Pooley D, Blackburne JA, Rappaport S, Schechter PL. 2007. *ApJ* 661:19–29
- 115. Pooley D, Rappaport S, Blackburne J, Schechter PL, Schwab J, Wambsganss J. 2009. *ApJ* 697:1892–1900
- 116. Refregier A. 2003. *ARAA* 41:645–668
- 117. Renzini A. 2006. *ARAA* 44:141–192
- 118. Riechers DA, Walter F, Brewer BJ, Carilli CL, Lewis GF, et al. 2008. *ApJ* 686:851–858
- 119. Riess AG, Macri L, Casertano S, Sosey M, Lampeitl H, et al. 2009. *ApJ* 699:539–563
- 120. Rusin D, Kochanek CS. 2005. *ApJ* 623:666–682
- 121. Saha P, Williams LLR. 2004. *AJ* 127:2604–2616
- 122. Saha P, Williams LLR. 2006. *ApJ* 653:936–941
- 123. Salpeter EE. 1955. *ApJ* 121:161–+
- 124. Salucci P, Lapi A, Tonini C, Gentile G, Yegorova I, Klein U. 2007. *MNRAS* 378:41–47
- 125. Sand DJ, Treu T, Ellis RS, Smith GP, Kneib JP. 2008. *ApJ* 674:711–727
- 126. Schneider P, Ehlers J, Falco EE. 1992
- 127. Schneider P, Kochanek CS, Wambsganss J. 2006
- 128. Schwab J, Bolton AS, Rappaport SA. 2010. *ApJ* 708:750–757
- 129. Shakura NI, Sunyaev RA. 1973. *A&A* 24:337–355
- 130. Springel V, Wang J, Vogelsberger M, Ludlow A, Jenkins A, et al. 2008. *MNRAS* 391:1685–1711

- 131. Stark DP, Swinbank AM, Ellis RS, Dye S, Smail IR, Richard J. 2008. *Nature* 455:775–777
- 132. Suyu SH, Marshall PJ, Auger MW, Hilbert S, Blandford RD, et al. 2010. *ApJ* 711:201–221
- 133. Suyu SH, Marshall PJ, Hobson MP, Blandford RD. 2006. *MNRAS* 371:983–998
- 134. Thomas J, Saglia RP, Bender R, Thomas D, Gebhardt K, et al. 2009. *ApJ* 691:770–782
- 135. Treu T, Auger MW, Koopmans LVE, Gavazzi R, Marshall PJ, Bolton AS. 2010. *ApJ* 709:1195–1202
- 136. Treu T, Ellis RS, Liao TX, van Dokkum PG, Tozzi P, et al. 2005. *ApJ* 633:174–197
- 137. Treu T, Gavazzi R, Gorecki A, Marshall PJ, Koopmans LVE, et al. 2009. *ApJ* 690:670–682
- 138. Treu T, Koopmans LV, Bolton AS, Burles S, Moustakas LA. 2006. *ApJ* 640:662–672
- 139. Treu T, Koopmans LVE. 2002a. *ApJ* 575:87–94
- 140. Treu T, Koopmans LVE. 2002b. *MNRAS* 337:L6–L10
- 141. Treu T, Koopmans LVE. 2004. *ApJ* 611:739–760
- 142. Treu T, Woo JH, Malkan MA, Blandford RD. 2007. *ApJ* 667:117–130
- 143. Trott CM, Treu T, Koopmans LVE, Webster RL. 2010. *MNRAS* 401:1540–1551
- 144. van Albada TS, Sancisi R. 1986. *Royal Society of London Philosophical Transactions Series A* 320:447–464

- 145. van der Wel A, Bell EF, van den Bosch FC, Gallazzi A, Rix HW. 2009. *ApJ* 698:1232–1243
- 146. Vegetti S, Koopmans LVE. 2009a. *MNRAS* 392:945–963
- 147. Vegetti S, Koopmans LVE. 2009b. *MNRAS* 400:1583–1592
- 148. Vuissoz C, Courbin F, Sluse D, Meylan G, Chantry V, et al. 2008. *A&A* 488:481–490
- 149. Warren SJ, Dye S. 2003. *ApJ* 590:673–682
- 150. Willis JP, Hewett PC, Warren SJ, Dye S, Maddox N. 2006. *MNRAS* 369:1521–1528
- 151. Winn JN, Rusin D, Kochanek CS. 2004. *Nature* 427:613–615
- 152. Wucknitz O, Biggs AD, Browne IWA. 2004. *MNRAS* 349:14–30
- 153. Xu DD, Mao S, Wang J, Springel V, Gao L, et al. 2009. *MNRAS* :1108–+
- 154. Yoo J, Kochanek CS, Falco EE, McLeod BA. 2006. *ApJ* 642:22–29

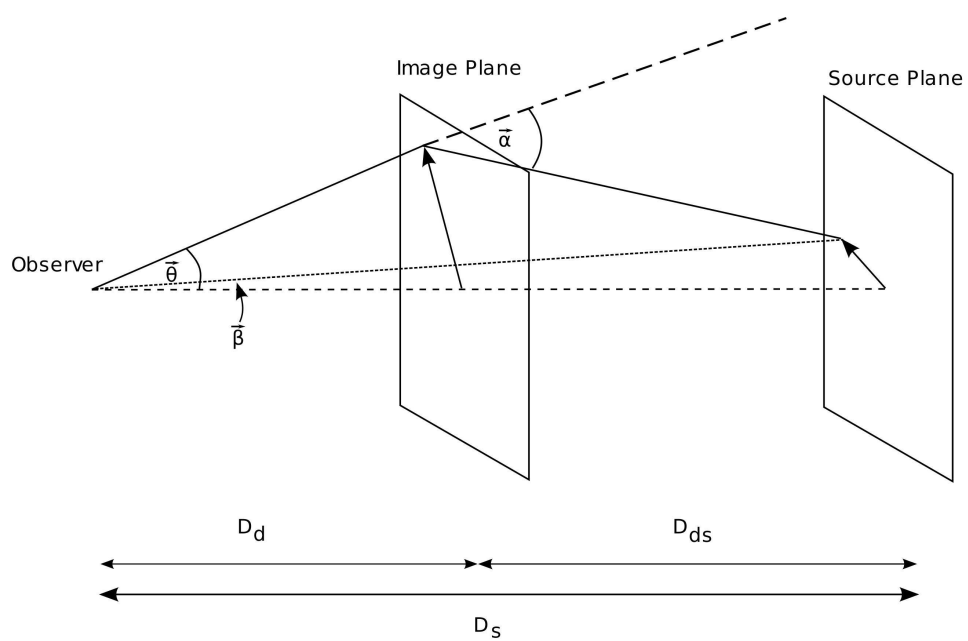


Figure 1: Sketch of the gravitational lensing geometry, courtesy of B.Brewer.



Figure 2: Examples of the most common configurations of galaxy-scale gravitational lens systems. A background source (top left) can produce four visible images (a “quad”; top right), an (incomplete) Einstein ring (bottom left), or two visible images (a “double”; bottom right), depending on the ellipticity of the projected mass distribution of the deflector and on the relative alignment between source and deflector (data from Moustakas et al. 2007, Image courtesy of P. Marshall).

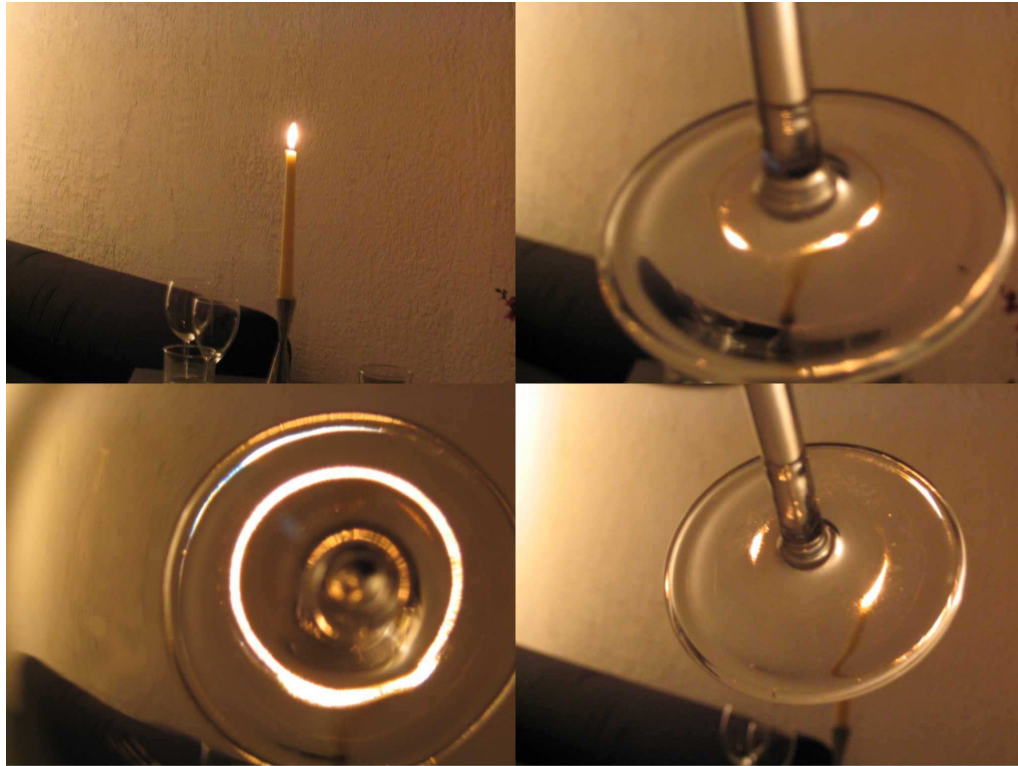


Figure 3: Optical analogy to illustrate the gravitational lensing phenomenon. The optical properties of the stem of a wineglass are similar to those of a typical galaxy scale lens. Viewed through a wineglass, a background compact source such as distant candle (top left), can reproduce the quad (top right), Einstein ring (bottom left), and double (bottom right) configurations observed in gravitational lensing and shown in Figure 2. Image courtesy of P. Marshall.

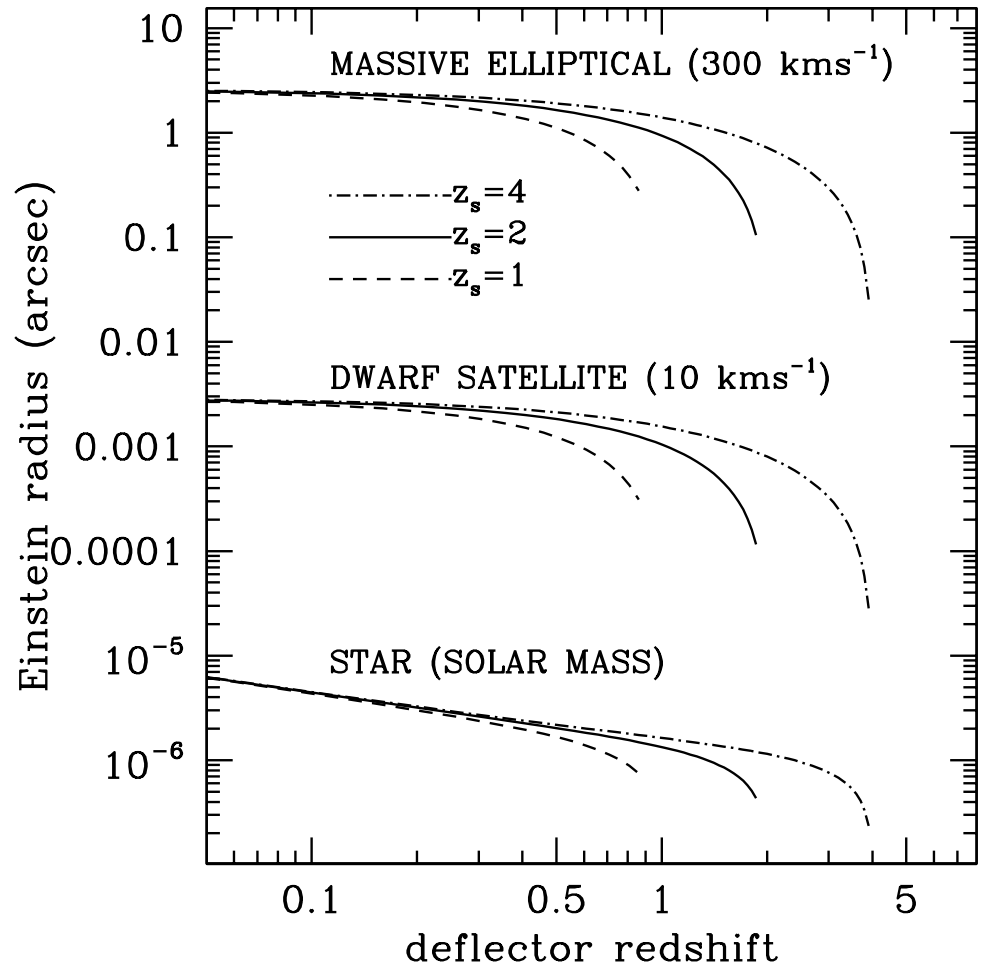


Figure 4: Einstein radius of a massive elliptical galaxy (top), a dwarf satellite (middle) and a star (bottom) as a function of deflector redshift for three choices of source redshifts ($z_s = 1, 2, 8$). SIS models with velocity dispersion $\sigma=300$ and 10 km s^{-1} are assumed for the elliptical and dwarf galaxies respectively. A point mass of one solar mass is adopted for the star.

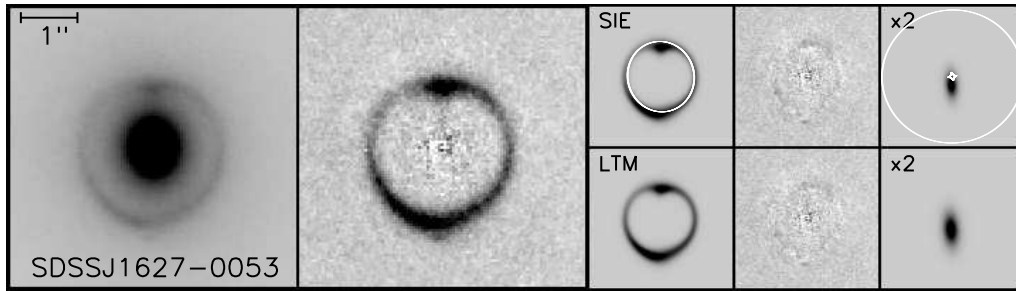


Figure 5: Example of a gravitational lens model, from Bolton et al. (2008a, reproduced by permission of the AAS). The two left panels show the data before and after subtraction of the light from the lens galaxy. The smaller panels on the right show the predicted image intensity of the best fit lens model, residuals, and source plane reconstruction, for an SIE mass model (top panels) and a mass traces light model (bottom panels). In the panel representing the image plane (labelled SIE) the white line shows the critical line. In the panel representing the source plane (magnified by a factor of 2) the white lines show the inner and outer caustics. Note that the peak of the surface brightness distribution is located outside the inner caustic and is therefore imaged twice, while the outer regions of the lensed sources go through the central region and therefore form an Einstein ring in the image plane.

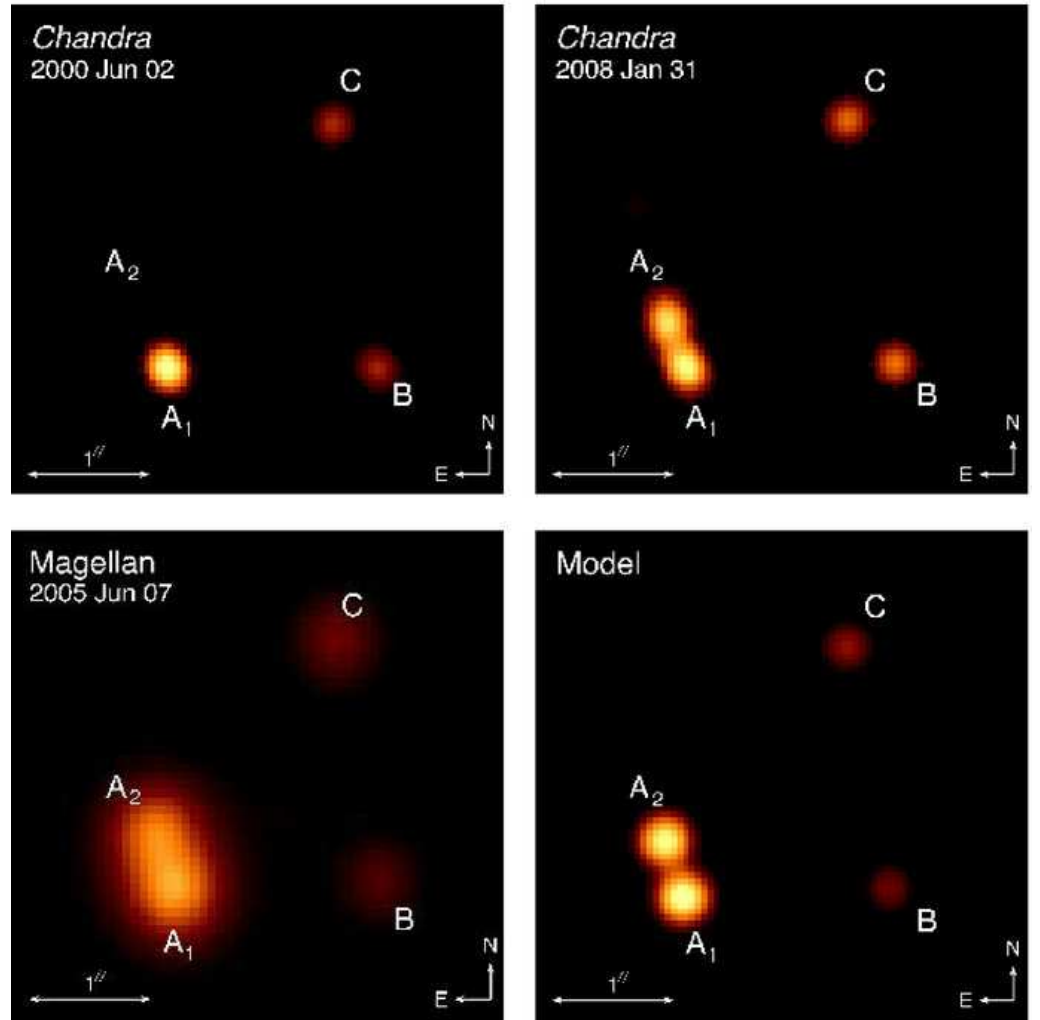


Figure 6: Microlensing observed in the quadruply-imaged quasar PG1115+080 ($z_s = 1.72$). The lens galaxy ($z_d = 0.31$) has been removed for clarity. Each panel is 4 arcseconds on a side. The bottom right panel (labelled Model) shows the expected image predicted from an SIS model of the deflector and an external shear term to account for the effects of a nearby group. The flux of image A₂ increased by over a factor of four between June 2000 and January 2008 (Figure from Pooley et al. 2009, reproduced by permission of the AAS).

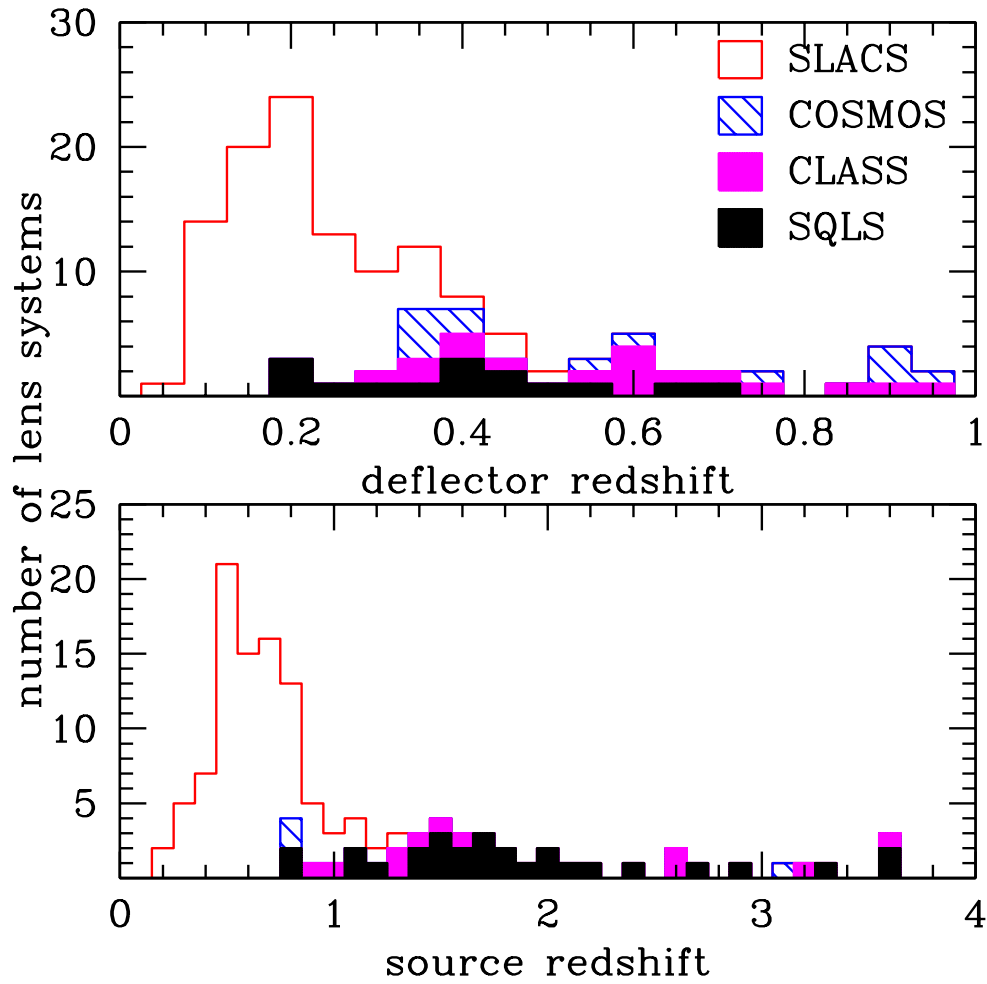


Figure 7: Distribution of deflector (top) and source (bottom) spectroscopic redshifts for the galaxy-scale gravitational lens systems discovered by the CLASS, COSMOS, SLACS, and SQLS surveys (see text for details).

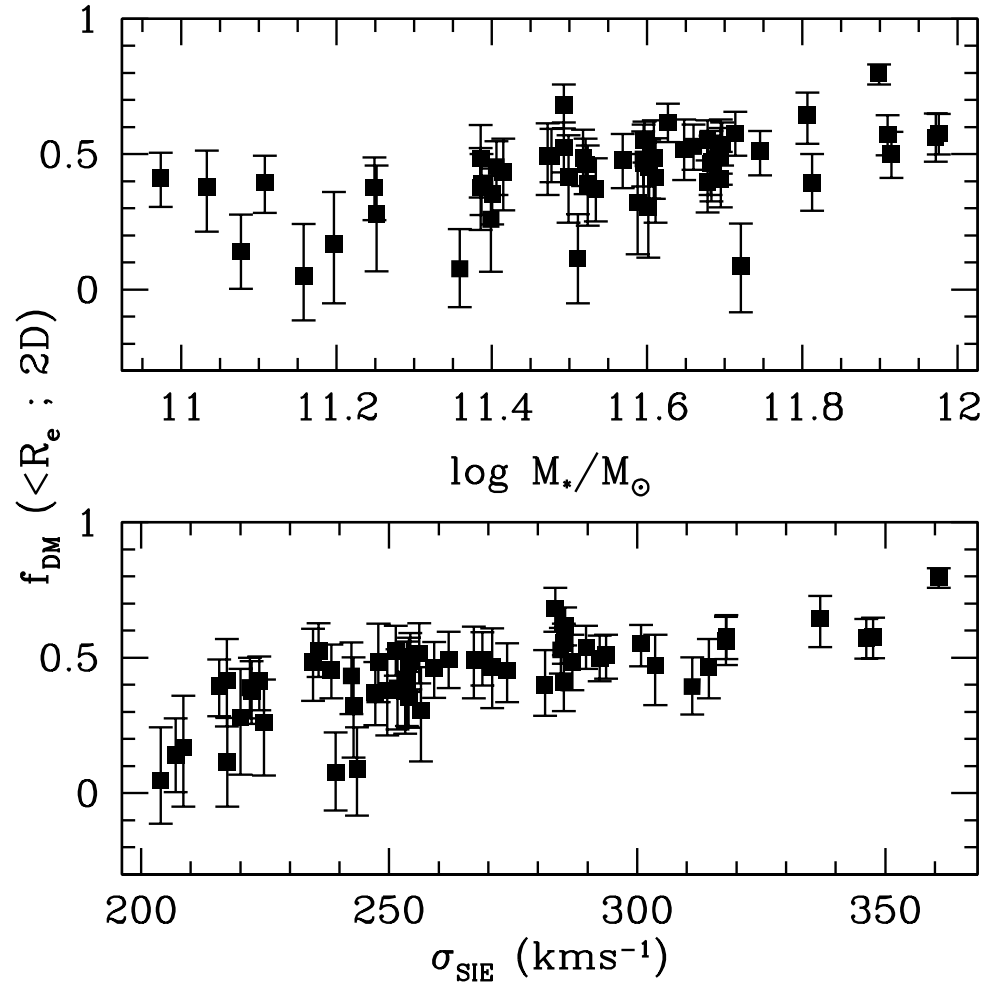


Figure 8: Dark matter fraction inside the cylinder of projected radius equal to the Einstein radius as inferred from stellar population synthesis modeling of multicolor data and strong gravitational lensing analysis of the SLACS sample (data from Auger et al. 2009).

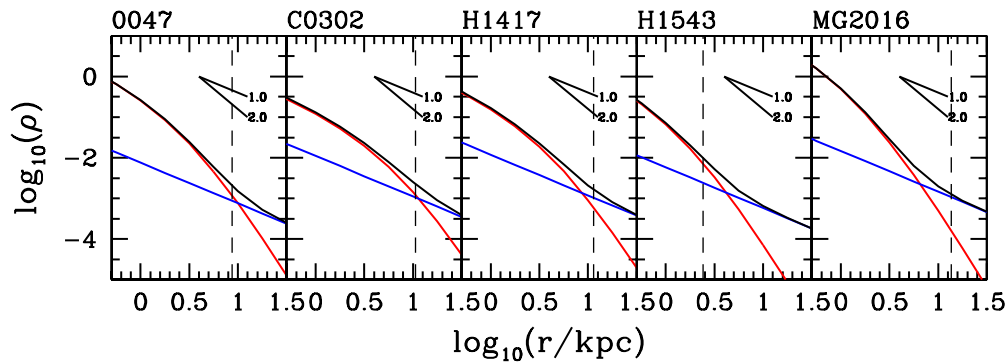


Figure 9: Mass density profiles of lens galaxies inferred from a strong lensing and dynamical analysis (Figure from Treu & Koopmans 2004, reproduced by permission of the AAS). In addition to the mass associated with the stars (red line), the data require a more extended mass component, identified as the dark matter halo (blue line). Although neither component is a simple power-law, the total mass profile is close to isothermal, i.e. $\gamma' = 2$. The vertical dashed line identifies the location of the Einstein radius.

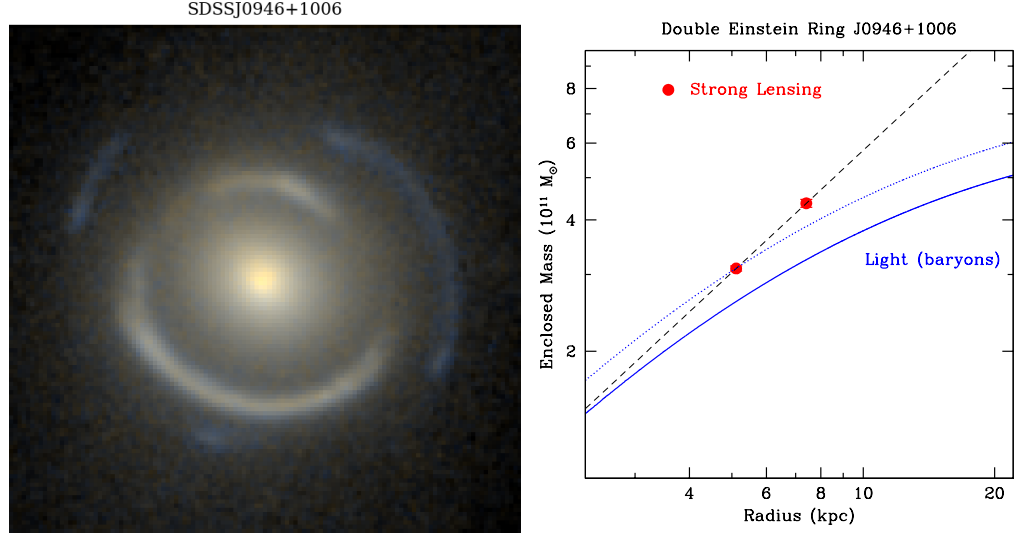


Figure 10: Double Einstein ring compound lens SDSSJ0946+1006. **Left:** color composite HST image (Courtesy of M. W. Auger). Note the foreground main deflector in the center, the bright ring formed by the images of the intermediate galaxy, and the fainter ring formed by the images of the background galaxy lensed by the two intervening objects. **Right:** Enclosed mass profile as inferred from the Einstein radii of the two rings (red solid points - the error bars are smaller than the points). The enclosed mass increases more steeply with radius than the enclosed light (solid blue line; rescaled by the best fit stellar mass-to-light ratio), indicating the presence of a more extended dark matter component. Even a “maximum bulge” solution (dotted blue line) cannot account for the mass at the outer Einstein radius.

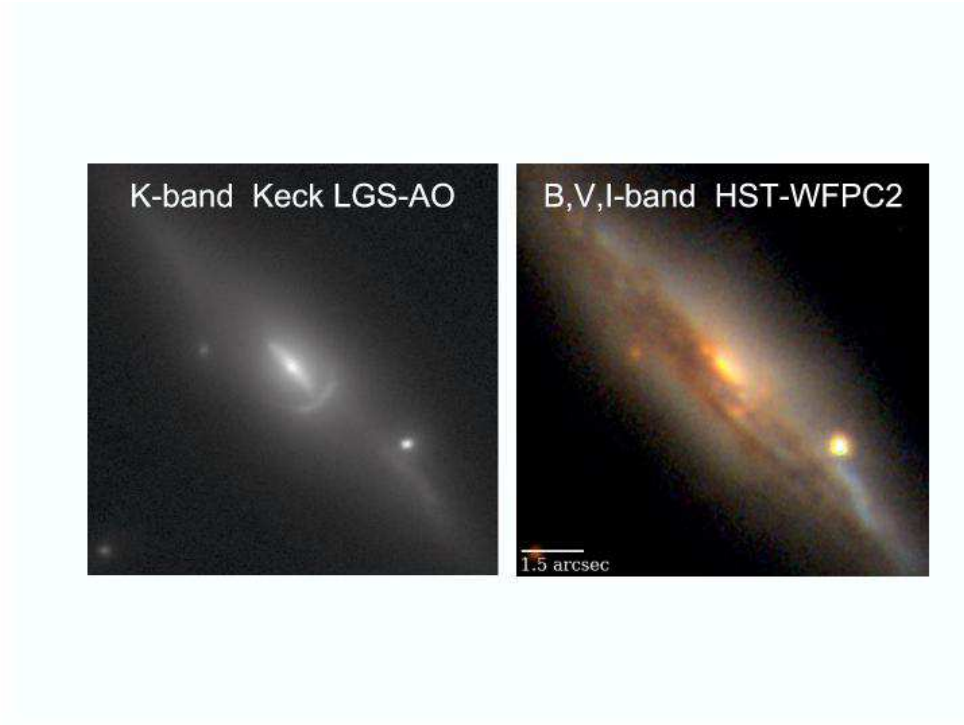


Figure 11: Example of edge-on spiral lens system ($z_d = 0.063$) discovered by the SWELLS Survey. The multiply-imaged source ($z_s = 0.637$) is visible in the optical HST discovery image and readily apparent in the Keck near infrared image where the effects of dust are minimized. The combined information at multiple wavelengths allows one to correct for dust and infer the stellar mass of the disk (Image credits: A. Dutton, P. Marshall, T.Treu).

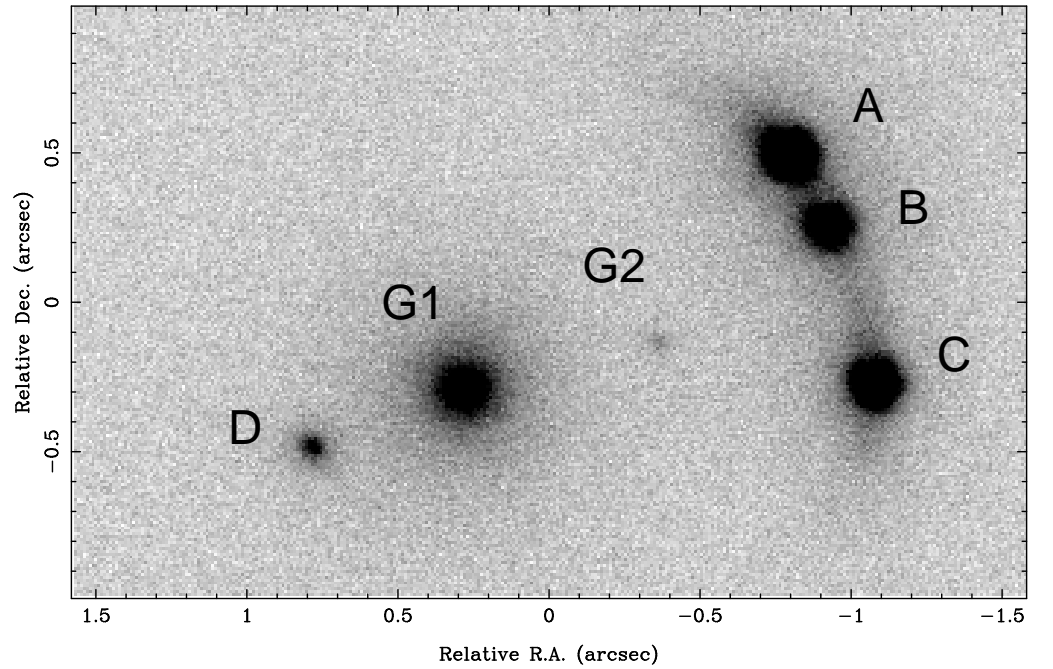


Figure 12: Near infrared ($2.2\mu\text{m}$) image of the gravitational lens system B2045+265 taken with the adaptive optics system at the 10m Keck-II Telescope (from McKean et al. 2007). For this kind of configuration, the flux of image B is expected to be equal to the sum of the fluxes of images A and C, in the absence of substructure (Bradač et al. 2002; Keeton, Gaudi & Petters 2003). The anomaly was originally discovered on the basis of radio images, ruling out microlensing or differential interstellar medium scattering as alternative interpretation (Fassnacht et al. 1999, Koopmans et al. 2003a). A satellite galaxy (G2) of the main deflector (G1) is detected in this deep and high resolution image. A small mass located at the position of the satellite can explain the observed anomaly.

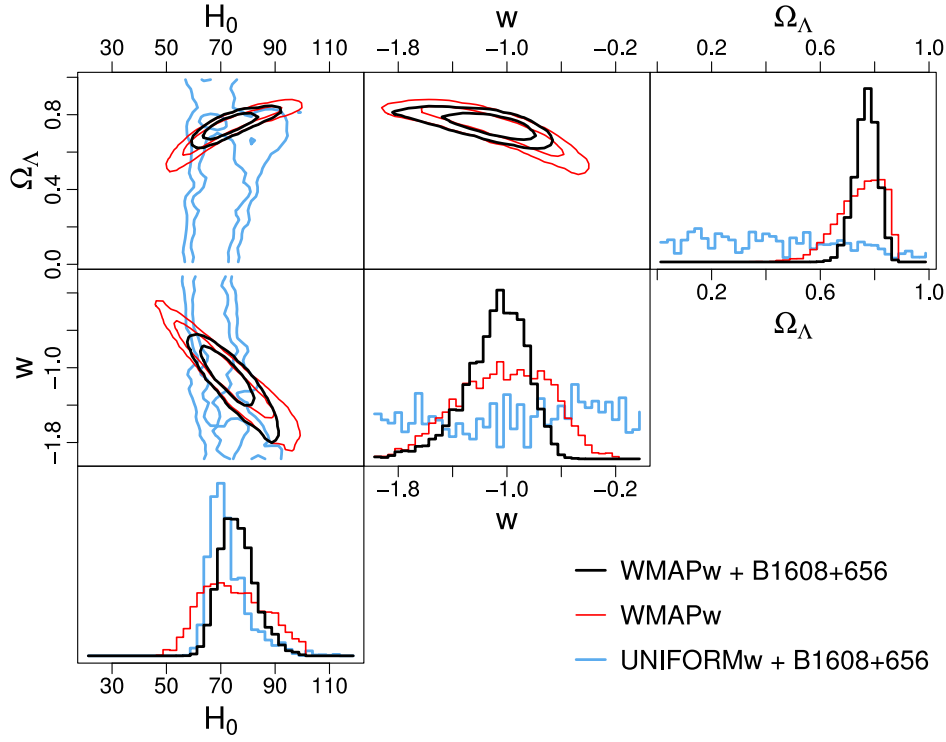


Figure 13: Illustration of cosmography with gravitational time delays. The panels show two and one dimensional posterior probability distribution functions for H_0 , w , and Ω_Λ , assuming flatness. Red lines indicate limits from cosmic microwave background, blue lines represent limits obtained from a single gravitational lens system with measured time delays (B1608+656), while black lines represent the joint constraints. Note how the constraints from time-delays are almost vertical in H_0 and therefore help break the degeneracy between w and H_0 in the CMB data. Lensing constraints in the $w - \Omega_\Lambda$ are broad and therefore not shown for clarity (Figure courtesy of S.Suyu; Figure from Suyu et al. 2010) .

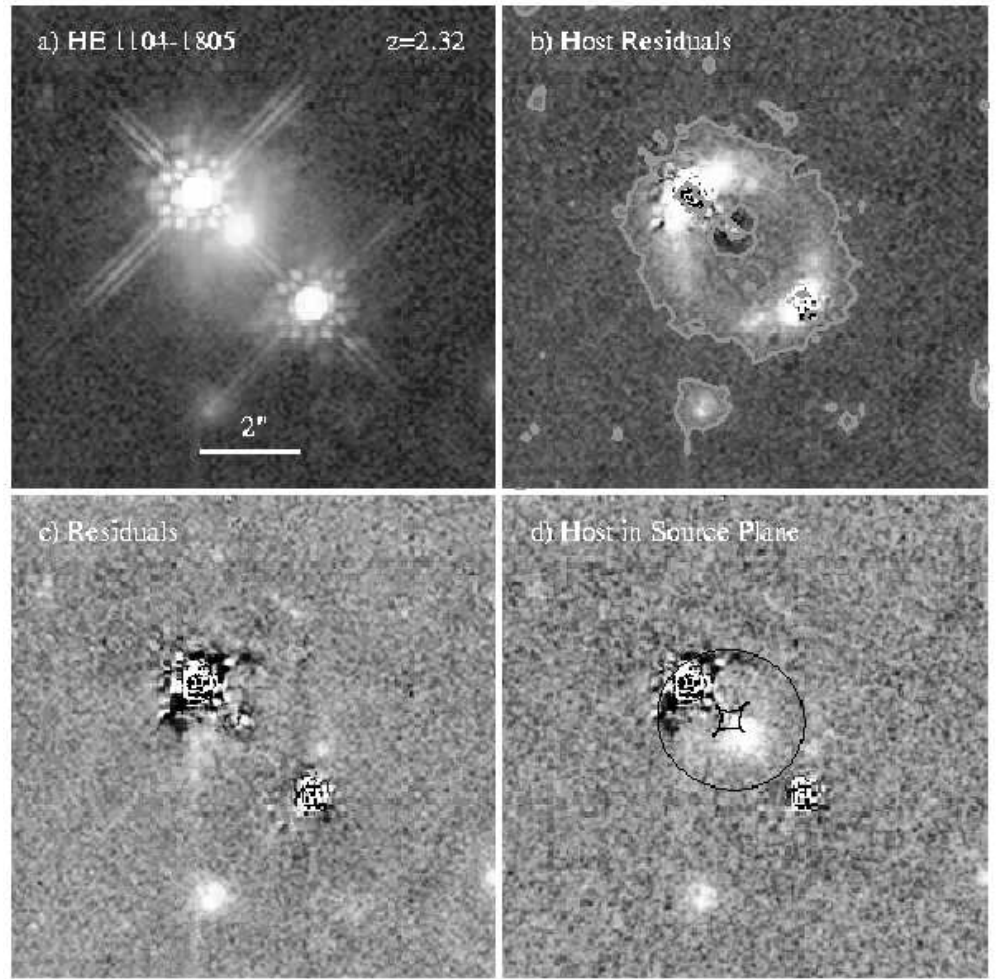


Figure 14: Illustration of gravitational lenses as cosmic telescopes. Two-image lens system (HE 1104-1805) of a $z_s = 2.32$ quasar produced by a $z_d = 0.73$ foreground galaxy. Panel a) shows the original data, panel b) shows the lensed host galaxy found after subtracting the deflector and quasar components of the best-fitting photometric model, panel c) shows the residuals from that photometric model, and panel d) shows what the unlensed host galaxy would look like in a similar exposure after perfectly subtracting the flux from the quasar. The curves shown superposed on the model of the host galaxy are the lensing caustics. (Figure from Peng et al. 2006, reproduced by permission of the AAS)